2018-12-12

A Study on Pile Setup of Driven Steel Pipe in Edmonton Till

Ni, Jiachen

UNIVERSITY OF CALGARY

A Study on Pile Setup of Driven Steel Pipe in Edmonton Till

by

Jiachen (Jason) Ni

A THESIS

SUBMITTED TO THE FACULTY OF GRADUATE STUDIES

IN PARTIAL FULFILMENT OF THE REQUIREMENTS FOR THE

DEGREE OF MASTER OF ENGINEERING

GRADUATE PROGRAM IN CIVIL ENGINEERING

CALGARY, ALBERTA

DECEMBER, 2018

ABSTRACT

As one of the major deep foundation types, driven steel pile (DSP) is widely used in all construction projects in Canada. Especially in rural northern Alberta areas where concrete supply is not accessible in a cost-effective manner, DSP foundation is highly preferred by heavy industrial development such as oil and gas related facilities.

For driven steel pile set in the fine-grained soils, significant pile-soil setup (pile capacity gain) is expected due to excessive pore water pressure dissipation after the pile installations. In the field, pile appeared to have a much lower capacity at the end of the installation compared to long-term performance. In a fast-paced construction environment, the time cost to wait and verify the pile long-term capacity is not desired. To proceed the upper structure construction without any delay, a reasonable prediction of DSP setup is required. Extensive research has been conducted to explain the mechanism and magnitude of the pile-soil setup effect. However, very limited study has been done on the rate / time of pore water pressure dissipation in clayey soils.

This study is aimed to provide a case study of the pile setup effect of DSP set in Edmonton clay till by using dynamic load testing, and wave equation analysis methods. A finite element numerical model is built to illustrate the pore water pressure dissipation and increase in radial effective stress, and allow geotechnical engineer to assess the pile setup behaviour with available soil testing results and reasonable assumptions.

ACKNOWLEDGEMENTS

I would like to thank the following people who have influenced this research project in some way:

Professor Ron Wong for his patience, wisdom and valuable guidance throughout the preparation of this thesis.

Mohamed El-Marassi, Ph.D., P.Eng. and Mark Brotherton, P.Eng. of Parkland Geotechnical Consulting Ltd. for supporting the resources of this project.

Dr. Xu Gong and Dr. Qiang Chen for their specialized knowledge about numerical modelling of geotechnical problems.

My mother who always remind me the importance of higher education.

Finally, my wife Jenny, for her enormous patience and support during my study.

TABLE OF CONTENTS

ABSTRACT i
ACKNOWLEDGEMENTS ii
TABLE OF CONTENTS iii
LIST OF FIGURES v
LIST OF SYMBOLS, ABBREVIATIONS AND NOMENCLATURE vi
1.0 INTRODUCTION 1
1.1 BACKGROUND 1
1.2 OBJECTIVES OF STUDY 2
2.0 LITERATURE REVIEW OF PILE SETUP IN CLAYEY SOIL 3
3.0 GENERAL SITE INFORMATION AND GEOLOGY 5
3.1 SITE LOCATION 5
3.2 LOCAL GEOLOGY 5
3.3 PILE FOUNDATION INFORMATION 5
4.0 SOIL PROPERTIES 8
4.1 FIELD GEOTECHNICAL INVESTIGATION 8
4.2 LABORATORY TESTING RESULTS 9
5.0 FIELD OBSERVATION OF DRIVEN STEEL PILES 17
5.1 WAVE EQUATION ANALYSIS (WEAP) PROGRAM WITH BLOW COUNT RECORD 17
5.1.1 Installation Blow Count Record 17
5.1.2 WEAP - Governing Equations and Numerical Scheme 18
5.1.3 WEAP Pile Model 20
5.1.4 WEAP Hammer Model 20
5.1.5 WEAP Soil Model 20
5.1.6 WEAP Bearing Graph Analysis 21
5.2 DYNAMIC TESTING METHOD OF PILE CAPACITY 22
5.2.1 Background 22
5.2.2 Wave Mechanics 23
5.2.3 Case Method and CAPWAP 23
5.3 ILLUSTRATIVE EXAMPLE 27
5.3.1 WEAP Analysis 27
5.3.2 Case Method and CAPWAP 29
5.4 PILE RESISTANCE ASSESSMENT 30
6.0 FINITE ELEMENT MODELING OF PWP DISSIPATION 44

6.1 CRYER EFFECT 44
6.2 NUMERICAL MODELLING OF PILE SETUP 44
6.2.1 Model Assumptions, Input and Soil Parameters 44
6.2.2 Element Type and Boundary Conditions 45
6.3 NUMERICAL MODELLING RESULTS AND COMPARISON 46
Pore Pressure Dissipation along the Pile Shaft 46
Pore Pressure Dissipation in Radial Direction 46
Induced Displacement Effect 47
Comparison between Field Data and FEM Results 47
7.0 SUMMARY 55
8.0 REFERENCES 1
9.0 APPENDIX – RESULTS OF UNDRAINED TRIAXIAL COMPRESSION TESTS 4

LIST OF TABLES

Table 4.1. Summary of In-situ Bulk Hydraulic Conductivity Testing 11
Table 4.2. Summary of Routine Soil Index Testing 11
Table 4.3. Summary of Consolidation Testing Results 11
Table 4.4. Summary of Triaxial Testing Results 12
Table 5.1. Recommended Quake and Damping Parameters in WEAP 32
Table 5.2. Summary of Observed Pile Setup 32
Table 6.1. Soil Parameters for Cryer Effect Model 48
Table 6.2. Soil Parameters for Cavity Expansion Model 48

LIST OF FIGURES

Figure 3.1. Site Location Map (Yellow Map, 2017) 6
Figure 3.2. Site and Pile Layout Plan Showing Studied 508-mm Piles 7
Figure 4.1. Borehole Log of BH16-04 13
Figure 4.2. Configuration of a Partially Perforated Well (Rice, 1976) 16
Figure 5.1. Flow Chart of Pile Setup Estimation 33
Figure 5.2. Wave Equation Models for Multiple Hammer Types (Hannigan, 1998) 34
Figure 5.3. Stress Strain Diagram of the Soil Resistance at a Pile Point (Smith, 1960) 34
Figure 5.4. Bearing Graph of a Pile at the Design Depth 35
Figure 5.5. PDA Sensors Mounting Diagram (ParklandGEO, 2018) 36
Figure 5.6. Force and Velocity Measurements from a Hammer Blow 36
Figure 5.7. Case Method – Relationship among Measured Forces, Velocities at Pile Top and Soil Resistance 37
Figure 5.8. SPTN and Undrained Shear Strength (S_u) of Clay 38
Figure 5.9. Unit Shaft Friction From WEAP and CAPWAP 39
Figure 5.10. Estimated Pile Resistance by Static Analysis versus PDA/CAPWAP at 20 m 40
Figure 5.11. CAPWAP Output Sample (ParklandGEO, 2018) 41
Figure 5.12. Pile Setup Percentage for 219-mm Diameter Piles 42
Figure 5.13. Pile Setup Percentage for 324-mm Diameter Piles 42
Figure 5.14. Pile Setup Percentage for 406-mm Diameter Piles 43
Figure 5.15. Pile Setup Percentage for 508-mm Diameter Piles 43
Figure 6.1. Pore Water Pressure After Applying a Surchage of 10 kPa 48
Figure 6.2. Pore Water Pressure After 1000 Days of Dissipation 49
Figure 6.3. Pore Water Pressure Dissipation vs Time 49
Figure 6.4. Schematic Diagram of Boundary Conditions for Cavity Expansion Model 50
Figure 6.5. In-situ Pore Water Pressure Distribution Prior to Cavity Expansion 50
Figure 6.6. Pore Water Pressure During Cavity Expansion At t = 0.01 hr 51
Figure 6.7. PWP Pressure Dissipation at Depth of 11 m (k=2e-10 cm/s) 52
Figure 6.8. Radial Effective Stress vs Pile Depth Along Shaft (k=2e-10 cm/s) 52
Figure 6.9. Pore Water Dissipation vs Radial Distance from Pile Location at Depth of 11 m (k=2e-10 cm/s) 53
Figure 6.10. Radial Effective Stress vs Radial Distance from Pile Location at Depth of 11 m (k=2e-10 cm/s) 53
Figure 6.11. Pore Water Dissipation with Different Induced Displacements 54
Figure 6.12. Pile Setup Percentage vs Time 54

LIST OF SYMBOLS, ABBREVIATIONS AND NOMENCLATURE

A_s	Pile shaft area	A_t	Pile toe area
A_c	Pile steel cross section area	E_p	Young's Modulus of pile steel
f_s	Unit shaft friction resistance	f_t	Unit toe bearing resistance
F_s	Total shaft friction resistance	F_t	Total toe bearing resistance
R_t	Total pile resistance	K_s	Soil stiffness
R_d	Dynamic pile resistance	DSP	Driven steel pile
R_s	Static pile resistance	B_c	Blow count
BOR	Beginning of restrike	PDA	Pile dynamic analysis
EOID	End of initial drive	CAPWAP	Case pile wave analysis program
WEAP	Wave equation analysis program	J	Soil damping factor
FEM	Finite element model	J_c	Case damping factor
c'	Apparent soil cohesion	q	Soil quake factor
S_u	Undrained soil shear strength	s	Pile permanent set (displacement)
kN	Kilo Newton's	v	Poisson's ratio
kJ	Kilo Jules	K	Permeability
u	Pore water pressure	ρ	Density
$\sigma_{v'}$	Vertical effective stress	γ	Unit weight of soil
$\sigma_{h'}$	Horizontal effective stress	DOS	Days of setup
E	Driving Energy (kJ or ft.lb)	C_c	Compression index
N	Blows per 0.25 m of pile penetration	m_v	Coefficient of compressibility
m	meter	u	Pile displacement from one hammer blow
s	second		
x	Pile section length	PWP	Pore water pressure
L	Radial distance from the pile location	D	Pile diameter
D_p	Vertical distance along the pile shaft	r	Pile radius

1.0 INTRODUCTION

1.1 BACKGROUND

It appears that Driven Steel Piles (DSP) installed in fine-grained soil would gain a significant amount of resistance after the initial installation and this behaviour is described as pile-soil setup effect. Typically, the percentage of pile setup typically ranges from 10% to 100% (Randolph, 1979) depending on the soil type and moisture condition. The main reason of this setup effect is that DSP installation would induce a radial displacement which generates excessive pore water pressures (PWP). This excessive PWP can be significant in fine-grained soils which have relatively low coefficients of permeability compared to coarse-grained soils. Based on the Theory of Effective Stress (Terzaghi, 1925), the effective strength of the soil around the pile shaft would decrease temporarily due to an increase in pore water pressure, but it will gradually get back to the original in-situ condition with the dissipation of excessive PWP.

In the construction field, pile installations are controlled and monitored by recording blow counts. In order to evaluate the blow count records, preliminary driving criteria should be developed (eg. Wave Equation Analysis Program (WEAP)). However, in the WEAP analysis, the assumption of pile-soil setup percentage (typically 30% for clayey soil based on software manual) is totally based on engineer's experiences and judgement. If actual pile setup percentage is much higher than that in the WEAP assumption, the final pile capacity after the setup would be underestimated based on the blow count records collected at the end of installation. Meanwhile, the most economical way to verify the final pile capacity probably is to re-tap the same pile and obtain additional blow count after a waiting period. Certainly, this method will still cause some delay in the foundation production since the primary installation equipment (hammer rig) will be used to verify the final pile capacity. With a better understanding of the pile setup percentage, setup up rate, and the relationship with soil parameters, the engineers could better assess the pile long-term performance and select the optimum pile re-tap time frame to speed up the foundation production.

1.2 OBJECTIVES OF STUDY

The objectives of this study are as follows:

- Perform a literature review of previous research on analytical and numerical study of pile setup effect.
- Review existing soil information including geotechnical investigation and soil laboratory testing results.
- Provide summary of field observations including pile installation records, dynamic pile load testing (PDA) results, and estimated pile capacity based on re-tap results.
- Perform numerical modeling on pore water pressure dissipation or consolidation after induced displacement of a soil mass.
- Compare and summarize the estimated pile setup gain from the field observations and numerical results.
- Propose an optimum time frame for final pile capacity verification of driven steel piles installed in Edmonton clay till.

2.0 LITERATURE REVIEW OF PILE SETUP IN CLAYEY SOIL

Extensive research has been conducted to explain the mechanism and magnitude of the pile-soil setup effect. Thixotropic and consolidation effects were proposed and studied (Farsakh, 2015) Soil aging and radial consolidation were also studied (Fakharian, 2013). Based on the available literature for piles driven in fine-grained clayey soils, the dominant mechanism for pile setup behavior is radial effective stresses increase due to dissipation of excessive pore water pressure induced by pile driving (Rosti, 2016).

Different approaches have been conducted to study the pile-soil setup. Visco-elastic consolidation model and equation was proposed and solved in finite difference method by Guo (2000). It is noted that the spring and dashpot soil model was adapted in Guo's research. Work-hardening soil model based on the critical state concepts (Roscoe, 1968) was proposed by Randolph (1979). In this paper, effects of over consolidation ratio due to soil stress history was studied for soil cavity expansion due to pile driving.

Finite element method (FEM) of pile driving was also used by several researchers to estimate the pile setup magnitude and compared to the field observations (Rosti, 2016). The anisotropic modified Cam-Clay model was adopted to describe the behavior of clayey soil. Cavity expansion was used in the FE model as the pile driving effect to the surrounding soils. Based on the available research findings, FEM modeling seems to be a feasible method to study the pore water pressure dissipation.

One extreme case will be pipe pile with soil plugging which would induce a much larger soil deformation during driving. FE analysis of this condition was studied by Ko (2016). A coupled Eulerian-Lagrangian (CEL) approach was applied to overcome the difficulties in the large deformation problems.

There are limited studies on the required time to achieve majority (eg. 90%) of the pile setup after the driving. In the field, the pile resistance increases is commonly estimated by using either static load testing or dynamic load testing methods. Pile Dynamic Inc. (PDI) introduced PDA testing for pile setup estimation (Rausche, 1985). Due to both static load test and dynamic load test were used as a "spot check" for individual pile capacity, a more generalized method was

proposed by Smith (1960) to model the pile driving as 1-D wave propagation along the pile shaft. Basically, a soil model consisted of spring and dashpot was proposed in Smith model. Lately, a commercial software GRLWEAP developed by GRL Engineers (2005) was widely accepted by geotechnical engineers to simulate the pile driving and resistance estimation based on blow count records. Some researcher pushed the study of pile setup time further by using piezometer installed along the pile shaft to measure the pore water pressure changes during and after the pile installations (Haque, 2014).

In terms of the setup percentage, Randolph (1979) proposed a ratio of 2 between final and initial radial effective stress which indicated 100 percent increase in resistance for Boston Blue Clay soil. Hydraulic conductivity of gravelly soils is quite high, therefore, the pile setup is considered to be negligible (about 10% or less).

3.0 GENERAL SITE INFORMATION AND GEOLOGY

3.1 SITE LOCATION

The clay / clay till deposits studied were found near Fort Saskatchewan, Alberta in a proposed petroleum industrial plant as shown in Figure 3.1. The local clayey soils are considered as a common soil type in Edmonton area.

This site is within Sturgeon County and surrounded by industrial plants and storage yards. The overall topography of this site was relatively flat.

3.2 LOCAL GEOLOGY

The information gathered through the field investigations at this site are consistent with the records of the Alberta Geological Survey. The upper sand that is near surface, is part of the aeolian sand dunes with minor loess typical of the local area. The underlying clay is consistent with Glacial Lake Edmonton deposits. The upper variation of clay till is consistent with Cooking Lake till, while the lower till appears to conform to Lamont glacial till. The larger layers of sand and silt in between the tills are consistent with Ministik Lake stratified sediments. The sand and gravel encountered at the terminating depths of boreholes in the investigation were similar to the Empress formation in a buried pre-glacial river valley. Deeper deposits would be the sandstone and siltstone bedrock of the Belly River formation (Andriashek, 1988).

3.3 PILE FOUNDATION INFORMATION

The foundation of the proposed petroleum plant consists of approximately 800 piles. The total area of the plant is about 300 x 400 m as shown in Figure 3.2. Piles consist of straight shaft open ended steel pipes with diameters and wall thicknesses of 219x9.5, 324x12.7, 406x12.7 and 508x12.7 mm sections. The pile embedment depths ranged from 12 m to 22 m. Figure 3.2 provides the site layout along with 508x12.7 mm piles installed which were either retapped or subjected to PDA and will be focused in this thesis. The pile spacings are so far apart that interference between piles is negligible.

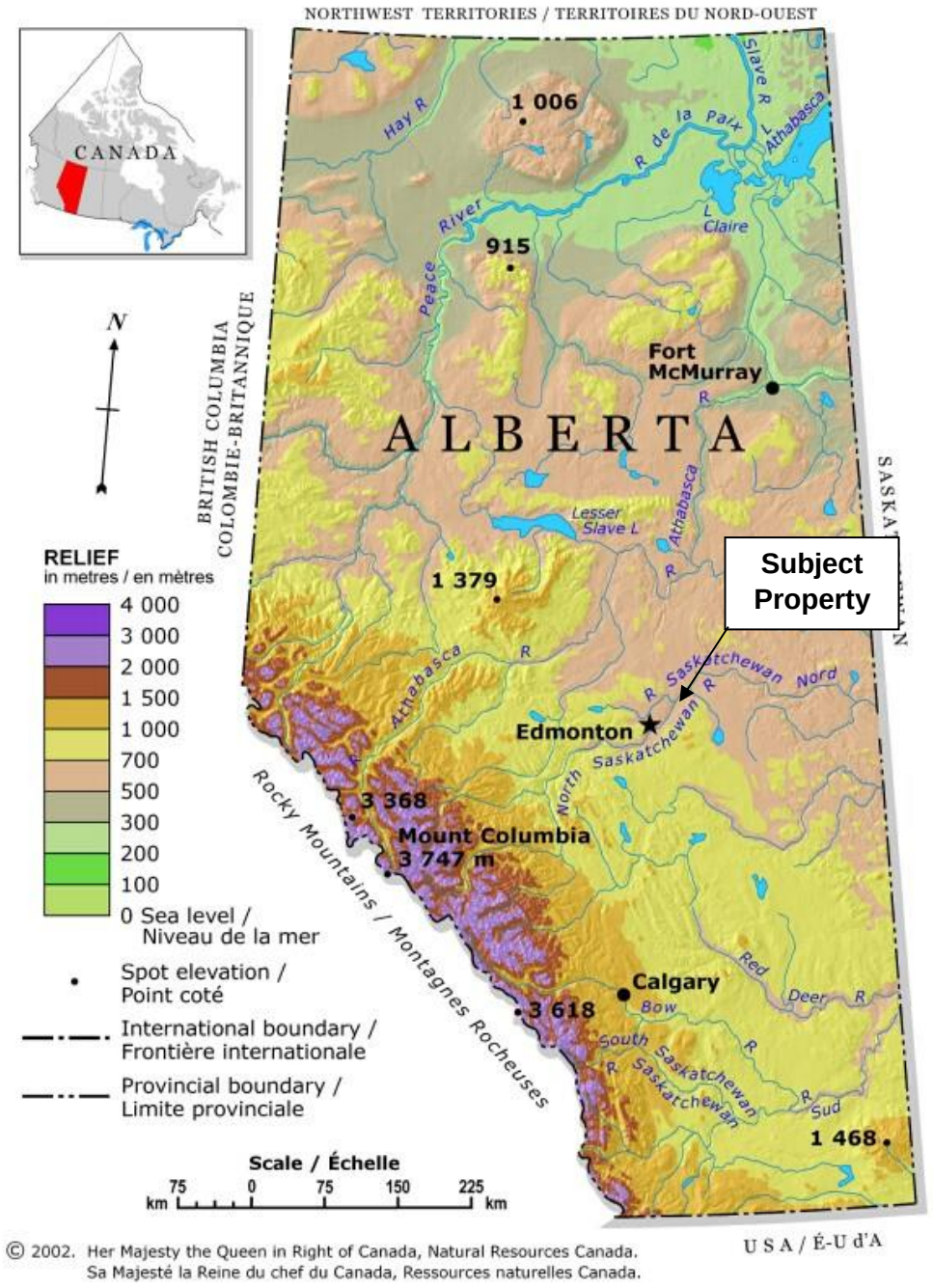

Figure 3.1. Site Location Map (Yellow Map, 2017)

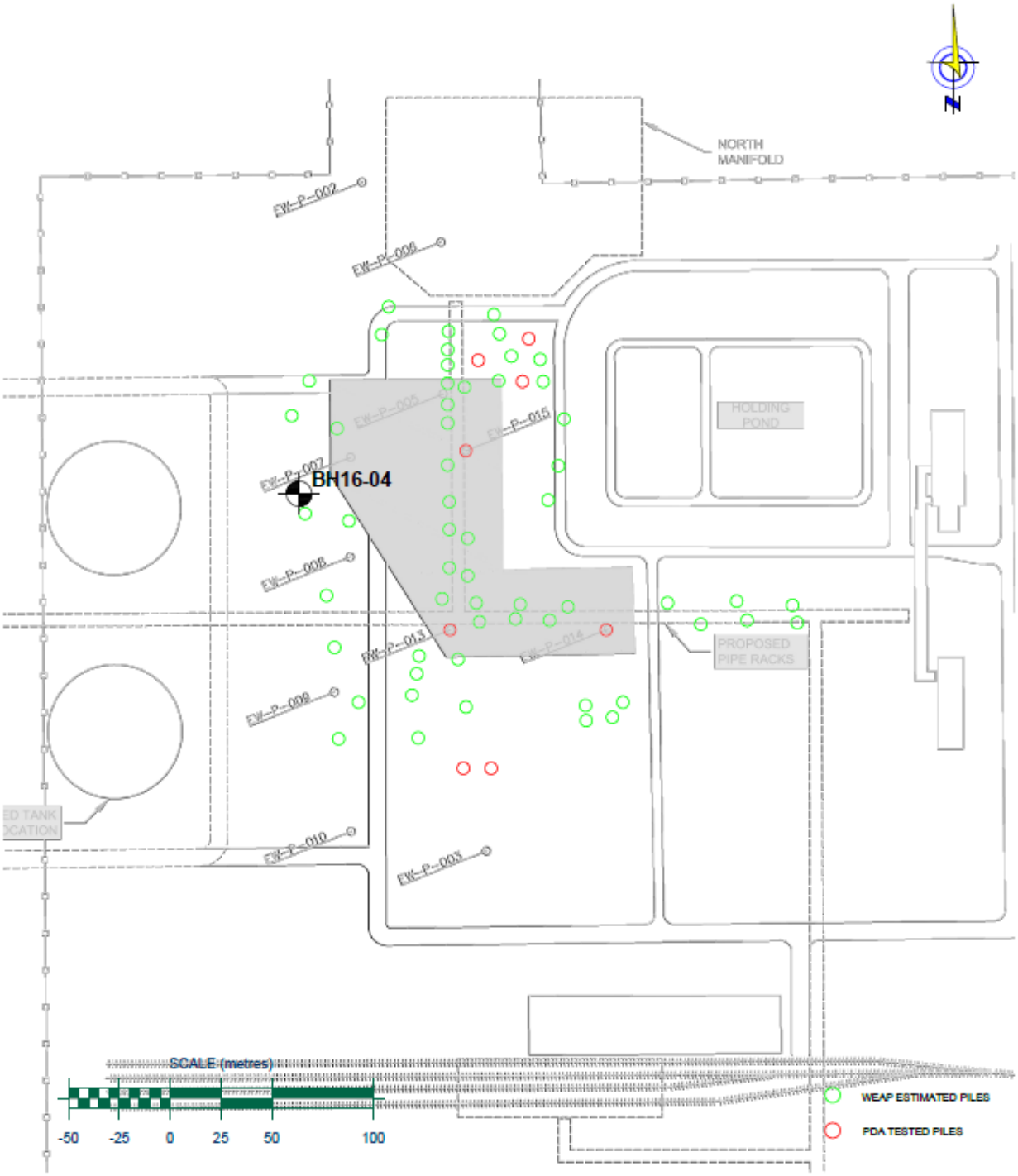

Figure 3.2. Site and Pile Layout Plan Showing Studied 508-mm Piles

4.0 SOIL PROPERTIES

4.1 FIELD GEOTECHNICAL INVESTIGATION

A geotechnical investigation program was carried out for this plant development project. Figure 3.2 indicated a relevant borehole drilled nearby the piling area (BH16-04). SPT "N" values ranged from 10 to 34 indicating a stiff to hard consistency. Detailed soil descriptions, SPT-N readings can be found in Figure 4.1: Borehole Log of BH16-04. Based on the field geotechnical investigation drilling findings, this Edmonton clay/clay till contained layers of sand or silt at varying elevations. The clay/clay till was brown to grey at relatively shallow depths (about 7 m) and generally contained some silt, little sand and trace gravel.

Moisture contents ranged from 13% to 39%, with an average of about 21%, which was considered above the Optimum Moisture Content (OMC). Based on the available triaxial test results, the saturated (bulk) density was found to have an average of 1976 kg/m^3 and an average dry density of 1548 kg/m^3. The clay was determined to be medium to high plastic with Atterberg liquid limits ranging from 33% to 63% and plastic limits ranging from 15% to 31% percent. Grain size analysis results indicated the clay contained 3% to 35% sand, 18% to 51% silt and 45% to 60% clay.

The ground water table measured during and after borehole drilling was between 1 to 2.5 m below grade. This ground water table was considered relatively shallow and the moisture contents of this clay indicated a saturated condition of this soil deposit.

In-situ bulk hydraulic conductivity testing was performed at Borehole 16-04 location at three depths in accordance with Bouwer and Rice method (Rice, 1976) which basically measures the displaced volume by injecting the water through a partially perforated well in unconfined aquifer. This method used a resistance-network analog to develop an empirical model for rate of water-level recovery during a slug test in an unconfined aquifer as shown in Figure 4.2. The solution is based on a constant-head boundary at the water table and the control well may be fully or partially penetrating. The Bouwer and Rice model assumes quasi-steady state flow by neglecting aquifer storativity. The governing equation proposed by Bouwer and Rice is provided as below:

$$\ln(H_0) - \ln(H) = \frac{2K_r Lt}{r_c^2 \ln(\frac{R_e}{r_w})} \quad (1)$$

where:

H = displacement at time t

H_0 = initial displacement at t = 0

K_r = radial (horizontal) hydraulic conductivity

L = screen length

r_c = nominal casing radius

r_w = well radius

R_e = external or effective radius of the test, typically, the length of the screen L

t = elapsed time since initiation of the test

A summary of some of the bulk hydraulic conductivity K_r results is presented in the Table 4.1.

4.2 LABORATORY TESTING RESULTS

Table 4.2 provides a summary of routine soil index testing results including Atterberg Limits and Soil Particle Analysis results. Based on particle size analysis results, the clay content for the subgrade soil up to 28 m ranged from 45.2 to 60.2 %, therefore, this clay deposit is considered as medium to high plastic.

Consolidation tests were undertaken on the clay and clay till samples and the results are summarized in Table 4.3. Reported test results included initial void ratio (e_i), compression index (C_c), hydraulic conductivity (k) and volume coefficient of compressibility (m_v). The measured k values from field slug tests and consolidation lab tests were slightly different which is probably attributed to the disturbance of soil sample in the lab condition.

Undrained consolidated triaxial compression test was conducted on the soil sample. The results of the triaxial testing are summarized in Table 4.4, and detailed results can be found in Appendix. The undrained shear strengths were obtained from the Shear Stress vs Normal Stress plot based on estimated effective normal stresses at the soil sample depths. The ratio of

undrained shear strength to effective normal stress is higher than 0.33 which indicates that the clay / clay till at this site were overly consolidated.

Based on the soil index tests, consolidation tests and consolidated undrained triaxial compression test results, the clay / clay till deposits at this site location is relatively consistent over the depth between 6 to 16 m. The hydraulic conductivities ranged between $2.8x10^{-9}$ and $4.4x10^{-10}$ cm/s and the apparent elastic modulus was about 16 MPa.

Table 4.1. Summary of In-situ Bulk Hydraulic Conductivity Testing

Depths (m)	Soil Type	Average Conductivity (cm/s)
6	Clay	8.1×10^{-10}
11	Clay Till	5.8×10^{-10}
28	Clay Till	6.9×10^{-10}

Table 4.2. Summary of Routine Soil Index Testing

Depths (m)	Soil Type	Percent Pass by Mass (%)				Plasticity (%)		
		Gravel	Sand	Silt	Clay	LL	PL	PI
6	Clay	0.0	9.7	30.1	60.2	63	31	32
11	Clay Till	0.0	3.1	50.6	46.3	39	18	21
28	Clay Till	1.0	35.2	18.2	45.2	33	15	18

Table 4.3. Summary of Consolidation Testing Results

Depths (m)	Soil Type	Test Results			
		e_i	C_c	k (cm/s)	m_v (m^2/MN)
6	Clay	1.0	0.3	2.4×10^{-9}	0.15
8	Clay Till	0.9	0.3	1.4×10^{-9}	0.10
16	Clay Till	0.5	0.1	6.9×10^{-10}	0.11

Table 4.4. Summary of Triaxial Testing Results

Sample Depth (m)	Soil Type	Shear Strength		Apparent Stiffness		Undrained Shear Strength (kPa)		
		Phi Angle Φ	Cohesion c' (kPa)	E_{50} (MPa)	E_{ur} (MPa)	σ'_v	S_u	S_u / σ'_v
10.7	Clay Till	27	17	16	48	103	60	0.58
						198	100	0.50
						398	170	0.43

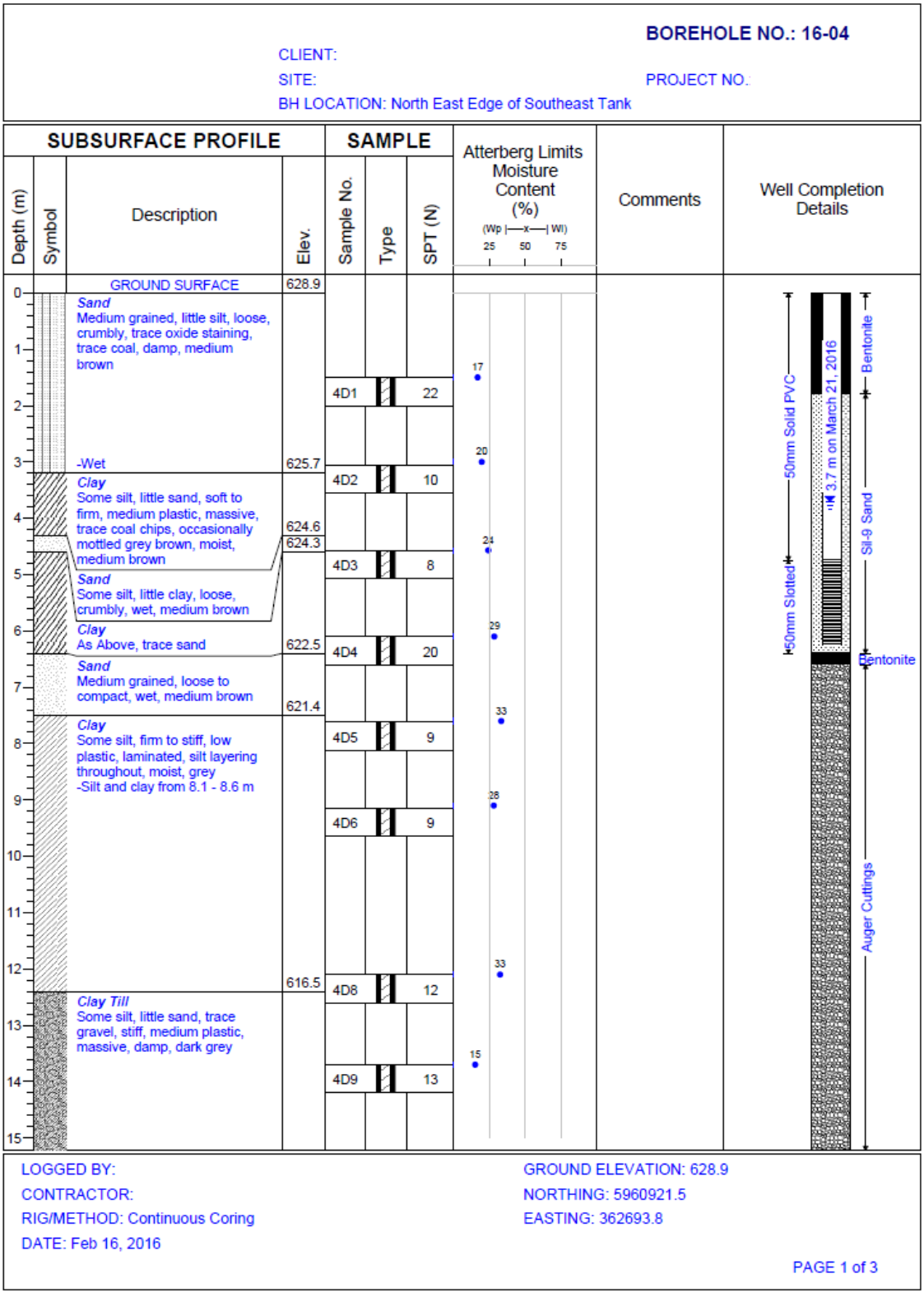

Figure 4.1. Borehole Log of BH16-04

BOREHOLE NO.: 16-04

CLIENT:

SITE

PROJECT NO.

BH LOCATION: North East Edge of Southeast Tank

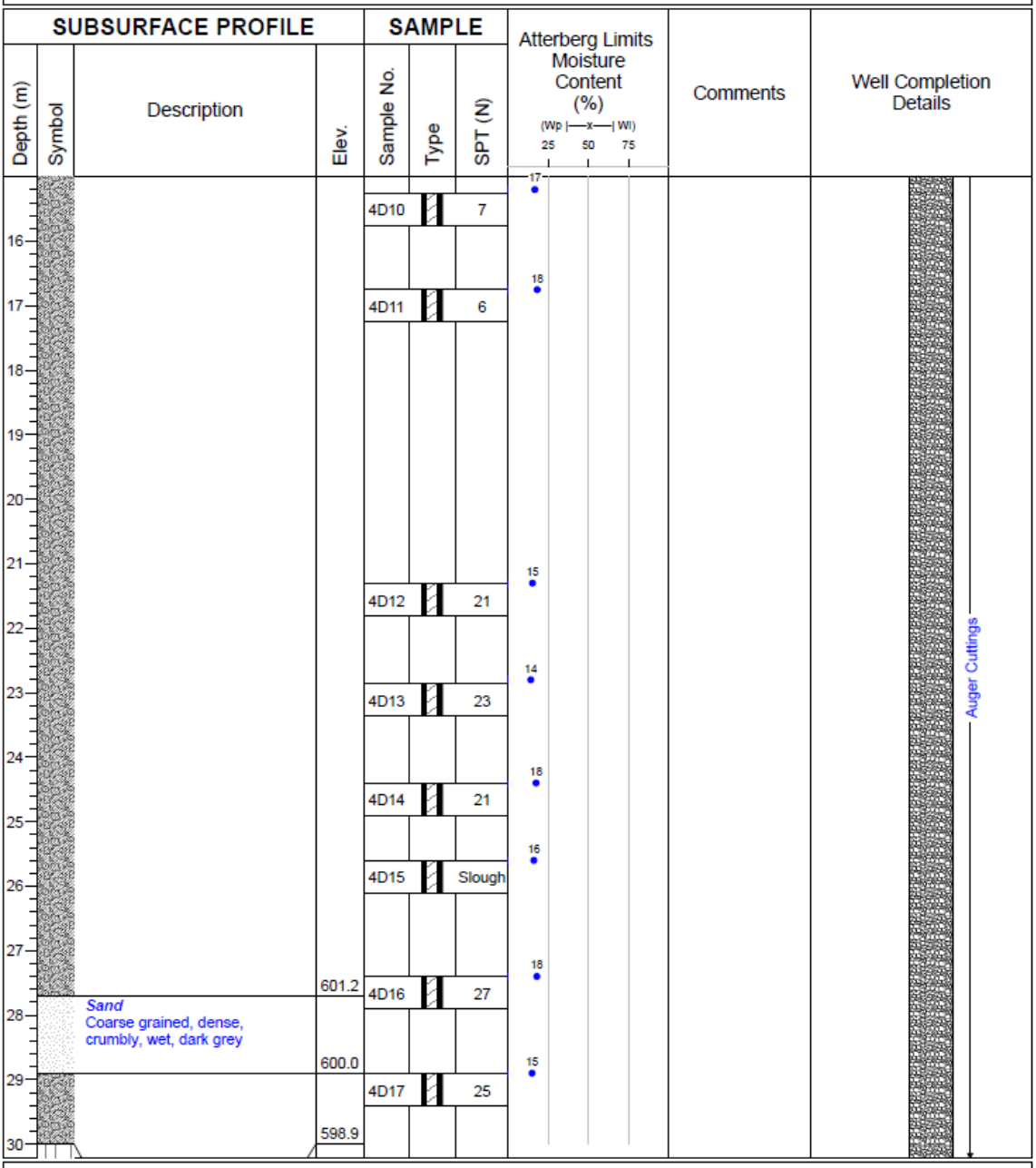

LOGGED BY:

CONTRACTOR:

RIG/METHOD: Continuous Coring

DATE: Feb 16, 2016

GROUND ELEVATION: 628.9

NORTHING: 5960921.5

EASTING: 362693.8

PAGE 2 of 3

BOREHOLE NO.: 16-04

CLIENT:

SITE: PROJECT NO.:

BH LOCATION: North East Edge of Southeast Tank

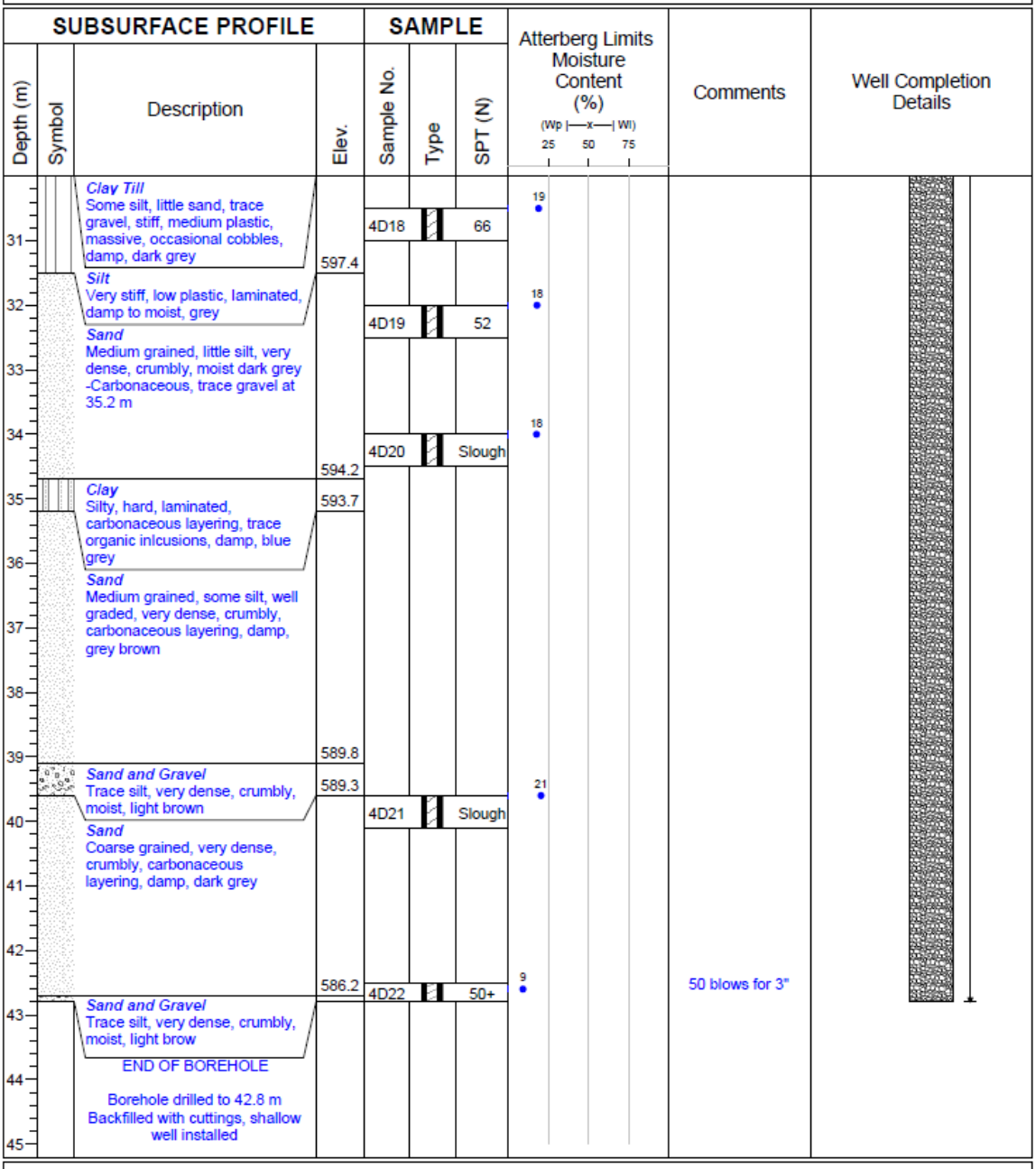

LOGGED BY:

CONTRACTOR:

RIG/METHOD: Continuous Coring

DATE: Feb 16, 2016

GROUND ELEVATION: 628.9

NORTHING: 5960921.5

EASTING: 362693.8

PAGE 3 of 3

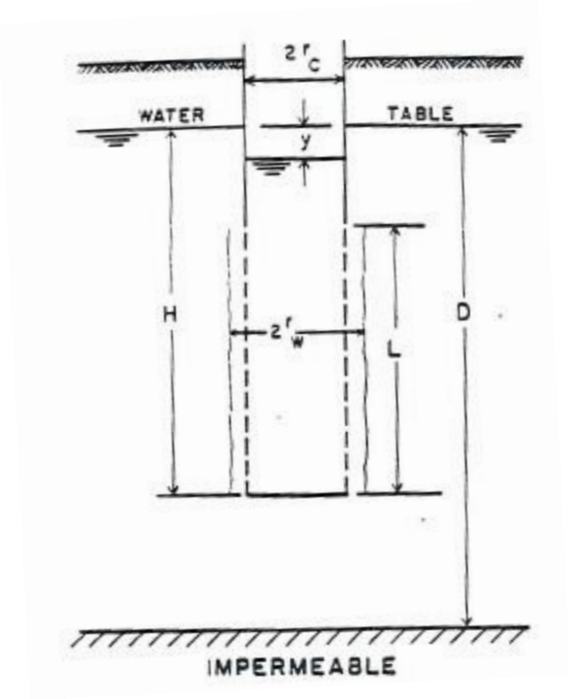

Figure 4.2. Configuration of a Partially Perforated Well (Rice, 1976)

Where:

y = displacement at time t

H = initial water level at t = 0

L = screen length

r_c = nominal casing radius

r_w = well radius

D = depth to impermeable layer

5.0 FIELD OBSERVATION OF DRIVEN STEEL PILES

In general, the magnitude and percentage of the pile setup effect are estimated from two methods:

1. WEAP analysis with blow count records.
2. PDA and CAPWAP with dynamic load testing data.

Figure 5.1 shows the flow chart outlining the procedures used in these two methods. Detailed procedures will be presented in the following sections. The pile capacity gain (pile setup effect) of 508-mm pile were estimated by these two methods and their locations are included in Figure 3.2.

5.1 WAVE EQUATION ANALYSIS (WEAP) PROGRAM WITH BLOW COUNT RECORD

5.1.1 Installation Blow Count Record

Before installation, piles were marked in 0.25 m (10”) intervals. Blow counts to penetrate each interval are recorded during the pile driving. Typical driving record contains the following information:

- Structure name and pile ID
- Date and time of the pile installation
- Pile size and total length
- Equipment (hammer model) and applied driving energy
- Final pile embedment depth
- Blow count for each interval
- Other field observations including pile plumbness, location offset, pile head condition, soil plug information etc.

5.1.2 WEAP - Governing Equations and Numerical Scheme

WEAP requires the modelling of hammer, driving system, pile, and soil as the inputs for wave equation analysis. A mathematical model using the one-dimensional wave equation was developed by Smith (1960). Similar to the Smith's model, WEAP models the hammer, the pile, and the soil resistance in a series of masses, springs, and viscous dashpots as shown in Figure 5.2. This program computes the pile driving blow counts, the axial driving stress on a pile, the hammer performance in terms of size and driving energy and estimated the pile resistances at different embedment depths. Two governing equations were given by Smith as below:

$$\rho \frac{\partial^2 u}{\partial t^2} = \frac{\partial}{\partial x} E_p \frac{\partial u}{\partial x} \pm R_t \qquad (2)$$

$$R_t = R_s + R_d = (u - u^p) K_s (1 + Jv) \qquad (3)$$

where:

ρ = density of steel pile, kg/m^3

u = displacement of pile, m

t = studied time, second

x = studied pipe section length, m

E_p = elastic modulus of steel pile, kPa

R_t = soil total static and dynamic resistance, kN

R_s = soil static resistance, kN ($= (u - u^p)K_s$)

R_d = soil dynamic resistance, kN ($= R_s J v$)

u^p = irrecoverable deformation / slip, and u^p = u-q, where q is "quake" as defined in Figure 5.3

K_s = soil stiffness, kN/m

J = soil damping constant at the point of the pile, s/m

v = velocity for pile element m, at time t, m/s

Based on the Smith model, during the impact, the force travels along the pile and bounces back from the pile toe, a time period could be divided into small intervals for step-by-step calculations. The hammer impact would generate a velocity and a displacement in the individual pile intervals (sections/elements) and weights. The displacement of two adjacent pile sections produces a compression / tension force in the spring between them. The force of two springs of the pile

sections will be partially overcome by the soil resistance and the net force will push the pile to a deeper embedment depth until the velocity becomes zero. This process is repeated for each soil section based on the following explicit finite difference numerical scheme for wave equation analysis until velocity reaches zero:

$$u(m,t) = u(m,t-\Delta t) + \Delta t\, v(m,t-\Delta t) \quad (4)$$

$$C(m,t) = u(m,t) - u(m+1,t) \quad (5)$$

$$F(m,t) = C(m,t)K(m) \quad (6)$$

$$R(m,t) = [u(m,t) - u^p(m,t)]K_s(m)[1 + J(m)v(m,t-\Delta t)] \quad (7)$$

$$v(m,t) = v(m,t-\Delta t) + [F(m-1,t) + M(m)g - F(m,t) - R(m,t)]\frac{\Delta t}{M(m)} \quad (8)$$

where:

m = pile section/element

t = studied time, s

Δt = time interval/increment, s

u = displacement for pile section/element m

v = velocity for pile element m, at time t, m/s

C = compression for pile element (pile internal spring) m, at time t, m

F = force for pile element (pile internal spring) m, at time t, kN

K = pile stiffness, kN/m

R = soil total static and dynamic resistance for pile element m, at time t, kN

u^p = irrecoverable deformation/slip for pile element, m, and u^p = u-q, where q is "quake" as defined in Figure 5.3

M = mass of pile element m, kg

The boundary conditions of the above numerical procedures consist of initial hammer impact force, and zero final pile velocity. The following minimum time interval is required to ensure stability in WEAP computations (Ng, 2011).

$$\Delta t = \frac{\Delta L/c}{1.6} \quad (9)$$

where:

c = velocity of wave propagation in the pile (wave speed of steel) (= $(E_p / \rho)^{1/2}$), m/s

ΔL = pile element length, m

5.1.3 WEAP Pile Model

In the WEAP program, pile model consists of following parameters:

- Pile unit weight, kN/m^3
- Pile cross section area A_c, m^2
- Pile total length and embedment depth, m
- Pile material modulus of elasticity E_p, MPa
- Compressive wave speed of pile material (steel) c, m/s

5.1.4 WEAP Hammer Model

The WEAP program contains a large data base of all types of hammers including drop hammers, hydraulic hammers and diesel hammers for DSP installations. A custom hammer option is also available to allow any modifications made for the existing hammer for certain pile installations. Below are the hammer parameters used in WEAP.

- Hammer ram weight, kg
- Hammer total weight including cushions, lead and helmet, kg
- Hammer stroke / ram drop height, m
- Maximum rated hammer driving energy, kJ

5.1.5 WEAP Soil Model

In the WEAP program, Smith's approach was used to model the surrounding soil with springs (quake) and dashpots (damping) as shown in Figure 5.2. Basically, quake is the required displacement to mobilize the soil resistance acting like a spring. Therefore, the mobilized resistance within the quake distance is the static resistance for the pile section. The soil spring constant K_s can be correlated to in-situ values of SPTN. Damping is the sensitivity of the material subject to impact velocity. For soils, soft soils tend to be more sensitive to impact speed compared to hard bedrock, therefore, clay has relatively high damping values. The damping and quake parameters of the soil model are typically assumed by engineer based on the values provided in Table 5.1 by GRLWEAP program.

In this WEAP analysis, the following soil parameters are required:

- Soil static spring constant K_s, kN/m
- Shaft damping constant J_s at each pile segment, s/m
- Toe damping constant J_t, s/m
- Shaft quake constant q_s at each pile segment, mm
- Toe quake constant q_t, mm

5.1.6 WEAP Bearing Graph Analysis

After entering all the pile, hammer and soil information, WEAP computes pipe displacement, velocity, internal, axial force, soil displacement, static and dynamic resistances along the pipe length as a function of time for a single blow from Equations (4) to (8). These results are used to determine the following information for the pile installation:

- Estimated pile resistance versus blow count relationship (bearing graph analysis)
- Blow count criteria with recommended driving energy for the design pile capacity
- Practical refusal criteria under hard driving condition
- Estimated driving stresses during installation
- Pile driveability study for proper hammer selection and energy settings

A bearing graph is a plot of estimated pile static resistance versus blow count as shown in Figure 5.4. The pile static resistance/capacity is estimated from the soil ultimate static resistance R_u (= q K_s) along all pipe elements for a single pile. The blow count is calculated from the following equation:

$$\frac{1}{B_c} = s = u_{toe} - q_t = \quad u_{toe} - \frac{\sum[R(m,t)q_x]}{R_t} \qquad (10)$$

where:

B_c = blow count, blow/m

s = permanent set, m/blow

u_{toe} = maximum toe displacement, m

q_t = average toe quake, m

q_x = individual quake for each pile segment, m

R(m, t) = maximum individual soil ultimate resistance of each pile segment at t*, kN

R_t = total soil ultimate resistance, kN

Since R(m, t) and R_t in Equation (10) are function of soil damping, thus, the bearing graph is dependent on the soil and toe damping constants, J_s and J_t. Figure 5.4 illustrates the bearing graph for a 508-mm pile with varying J_s of 0.6 – 1.0. For a given soil damping constant, the estimated blow count increases with increasing static pile capacity or soil resistance. In addition, the static pile capacity decreases with increasing soil damping constant.

5.2 DYNAMIC TESTING METHOD OF PILE CAPACITY

5.2.1 Background

It is understood that WEAP analysis program was used to estimate the pile resistances based on blow count records. However, this numerical analysis has some limitations, and following assumptions are generally applied to the WEAP study:

- Assumed soil damping and quake parameters for generalized soil profile which did not consider some localized soil variation.
- Uncertainty for driving energy of hammer

In reality, soil condition variation, cold weather, switching hammer helmet, cushion, out-dated hammer calibration, or possible alignment offset will all affect the blow count records during the pile installation. Hence, the pile resistances estimation based on WEAP analysis could be questionable. Therefore, dynamic pile load testing or Pile Dynamic Analysis (PDA) in accordance to ASTM D4945-17 (2017) is introduced to assess the in-situ pile resistances and verify the WEAP assumptions and criteria.

5.2.2 Wave Mechanics

For pile subjected to a hammer impact blow, the one-dimensional axial wave equation is given by:

$$\frac{\partial^2 u}{\partial t^2} = \frac{E_p A}{m_p}\frac{\partial u}{\partial x} \qquad (11)$$

Where:

m_p = pile section mass, kg

A = pile cross section area, m^2

$\frac{\partial u}{\partial x}$ = strain,

$\frac{\partial^2 u}{\partial t^2}$ = acceleration, m/s/s

When the pile section is subjected to a hammer blow, the initial and boundary conditions of this one-dimensional Wave Equation are as below:

- The initial acceleration (velocity) and strain (force) is zero.
- Induced strain and stress in the pile section due to hammer impact force.
- At the end of the hammer blow, acceleration (velocity) and strain (force) back to zero.

It is noted from Equation (11) that the left-hand side is the acceleration and the right-hand side is the pile strain which correspond to driving forces. The pile velocity (displacement /acceleration) is proportional to the driving force, therefore; this equation can be used to validate the computed results of pile displacement and induced hammer driving force.

5.2.3 Case Method and CAPWAP

Based on the Equation (11), it appears that acceleration $\partial^2 u/\partial t^2$ and strain $\partial u/\partial x$ are the only two variables and they are proportional to each other. Basically, a typical PDA testing would involve two accelerometers and two strain gauges, and they are attached to the H-pile shaft as shown in Figure 5.5 to account for hammer misalignment and possible sensor malfunctions. It is also recommended to place the sensors at least two pile diameters away from the pile top. A sample of measured force and velocity curves are provided in Figure 5.6.

Case method is a numerical technique used in the PDA to determine the static soil resistance (i.e., pile resistance). The Case method assumes a uniform cross section, linear, and elastic pile, which is subjected to one-dimensional axial load and is embedded in a perfectly plastic soil. Under a hammer impulsive load, the total static and dynamic soil resistance R_t acting on a pile can be estimated using Equation (12), for which the detailed derivation was reported in Rausche et al. (1985). Rausche et al. did not solve for the total pile resistance R_t from the dynamic equilibrium Equation (2) directly. Instead, they analysed how the pile resistances along the side and at the toe affect the wave propagation in the pile. With given pile parameters (E_p, A_c and ρ), the total pile resistance could be related to the measured velocity (acceleration), and measured force (strain) at a pile segment by adjusting soil static and dynamic properties (Rausche et al. 1985):

$$R_t = \frac{1}{2}[F_1 + F_2] + \frac{1}{2}[v_1 - v_2]\frac{EA}{c} \qquad (12)$$

where:

R_t = total pile resistance, kN

F_1 = measured force at time of initial hammer impact, kN

F_2 = measured force at time of reflection from pile toe, kN

v_1 = measured velocity at time of initial hammer impact t_1, m/s

v_2 = measured velocity at time of reflection from pile toe $t_2 = t_1 + 2L/c$, m/s

c = wave speed of steel, 5123 m/s

L = pile length, 20 m

E = modulus of elasticity of a pile material, 210000 MPa

A = pile sectional area, m^2

Because we are only interested in static pile resistance which is the typical loading scenario of a structure, static resistance must be separated from the total pile resistance based on the following equations (Rausche et al. 1985):

:

$$R_s = R_t - R_d \qquad (13)$$

$$R_d = J_c v_t \qquad (14)$$

where:

R_s = static pile resistance, kN

R_t = total pile resistance, kN

R_d = dynamic pile resistance, kN

J_c = Case damping factor, s/m

v_t = pile toe velocity, m/s; it is given by

$$v_t = 2v_1 - \frac{c}{EA}R_t \qquad (15)$$

Combining Equations (12), (13), (14) and (15), the maximum static resistance can be calculated based on the following equation (Rausche et al. 1985):

$$R_s = \frac{1}{2}\left\{(1-J_c)\left[F(t_m) + \frac{EA}{c}v(t_m)\right] + \frac{1}{2}(1+J_c)\left[F\left(t_m + \frac{2L}{c}\right) - \frac{EA}{c}v(t_m + \frac{2L}{c})\right]\right\} \qquad (16)$$

where:

t_m = time when maximum total resistance R_t, occurs or maximum force was transferred to the pile, s

$F(t_m)$ = measured force at pile top at time t_m, kN

$F(t_m + 2L/c)$ = measured force at pile top at time of reflection from pile toe $t_m + 2L/c$, kN

$v(t_m)$ = measured velocity at pile top at time t_m, m/s

$v(t_m + 2L/c)$ = measured velocity at pile top at time of reflection from pile toe $t_m + 2L/c$, m/s

c = wave speed of steel, 5123 m/s

L = pile length, m

The physics involved in Equations (12) and (16) is illustrated in Figure 5.7. The soil resistance calculation comprises the average of two measured forces at the pile top at a time interval of 2L/c and the average measured acceleration at the pile top over the same interval times the pile mass. This is simply analogous to the Newton's Second Law if the time interval approaches zero.

According to Rausche et al. 1985), the time t_m depends on the pile type. For displacement piles and piles with large shaft resistance, time t_m coincides with the time of initial hammer impact (first velocity peak). For end bearing piles, time t_m may occur at later time, which is verified by plotting the resistance with time. It is also important to make sure the maximum resistance is fully mobilized during the time interval of 2L/c.

It should be noted that the Case method mentioned above does not consider the soil profile and resistance distribution (layered system) nor the toe damping and quake. A signal matching computer program was developed by Professor Goble in the 1970s. It is a computer program to verify the pile static resistance with more accurate numerical estimation of the soil resistance distribution and dynamic soil parameters along the depth. This program called Case Pile Wave Analysis Program (CAPWAP) which applies a signal matching method.

Compared to the Static Load Testing method of pile foundation, the results of PDA testing and further CAPWAP analysis for the pile resistance estimation are relatively accurate based on some case studies provided by Likins (2004). As PDA is considered as direct measurement of individual pile capacity, it is more accurate than WEAP estimation which is only based on bearing analysis.

A PDA testing program was implemented before the construction stage at this site. The main purpose of this program was to verify the geotechnical recommendations for the DSP pile foundations. Pile unit skin friction and end bearing parameters were verified through this PDA testing program for different pile sizes and depths. Final pile foundation design was based on the findings of this testing program which includes two type of PDA testing:

- End of initial drive (EOID) test to assess the pile resistance along the driving. This is important to determine the approximate embedment depth to achieve the design pile capacity.
- Beginning of restrike (BOR) PDA testing to verify the final pile resistance after period of setup time.

5.3 ILLUSTRATIVE EXAMPLE

5.3.1 WEAP Analysis

In the WEAP program, the 508 mm pile model includes the following parameters:

- Pile unit weight: 77.5 kN/m^3
- Pile cross section area A_c: 197 cm^2
- Pile total length: 22 m and embedment depth L = 20 m
- Pile material modulus of elasticity, E_p = 210000 MPa
- Compressive wave speed of pile material (steel), c = 5123 m/s

Provided by the piling contractor, the following parameters were used for the DFI HH450 hydraulic hammer:

- Hammer ram weight: 4499 kg
- Hammer total weight: 6894 kg
- Hammer stroke: 1.75 m
- Maximum rated hammer driving energy: 77 kJ

The following dynamic soil parameters were applied in this WEAP for the 508 mm piles which were calibrated based on PDA and CAPWAP method.

- Shaft damping factor at each pile segment: 0.8 s/m
- Toe damping factor: 0.5 s/m
- Shaft quake at each pile segment: 2.5 mm
- Toe quake: 4.2 mm

The static soil analysis in the WEAP program was based on SPT-N values for the clay / clay till soils. The unit skin friction and end bearing values were calculated by using alpha method (CFEM, 2006) as below:

$$f_s = \alpha S_u = \alpha * SPTN * 9 \quad (17)$$

$$f_t = 9 * S_u = 81 * SPTN \quad (18)$$

$$R_s = F_s + F_t = f_s DL\pi + f_t \frac{1}{4} D^2 \pi \quad (19)$$

where:

p_s = unit skin friction, kPa

p_t = unit toe bearing, kPa

α = coefficient of pile skin friction for undrained cohesive soils, dimensionless

S_u = undrained shear strength, kPa

SPTN = standard penetration value, blows / 300 mm

F_s / F_t = accumulative pile shaft / toe resistance, kN

D = diameter of pile, m

L = embedment length of pile, m

With R_s calculated from Equation (19), the soil static spring constant K_s is defined by the quake value selected.

Based on SPTN values included in Borehole log BH16-04 provided in Figure 4.1, the SPTN and estimated undrained shear strength S_u versus depth is plotted in Figure 5.8. As per Figure 18.1 of CFEM (2006), the factor α was taken as 0.5 for fine-grained soil with an undrained shear strength of about 100 kPa. This average α value was used in calculation of unit shaft friction for static analysis, and the results are plotted in Figure 5.9. The unusually high values of SPTN at depths of 1.5 and 6 were readjusted in this plot.

The static resistance versus depth based on SPTN is plotted in Figure 5.10. The resistance increases at an approximately linear manner with depth, reflecting the uniform distribution of unit shaft friction along pile embedment length shown in Fig. 5.9.

After obtaining all the parameters for the pile, hammer, soil models, Equation (10) was solved in WEAP program by using numerical schedule provided in Section 5.1.2, and the blow count versus pile resistance plot is provided in Figure 5.4. Three damping factors of 0.6, 0.8 and 1.0 were used to evaluate the possible soil variation effects. It is noted that for higher damping values, higher blow count will be required to achieve the same pile resistance.

For this plant site, bearing graphs were obtained for all pile sizes, depths, and used to determine the pipe setup between EOID and BOR.

5.3.2 Case Method and CAPWAP

In this section, one of the 508-mm pile tested by PDA method will be illustrated. The measured force and velocity of this 508x12.7 mm pile subjected to a hammer blow was shown in Figure 5.6. The measured force and velocity respond at a same rate at the beginning as the pile top is exposed to air. When the wave enters the pile sections embedded in the soil, the measured force and velocity are reduced at different rates. The vertical distance between the measured force and velocity during the time interval of 2L/c and at time of reflection from the toe are measures of the soil shaft and toe resistances mobilized, respectively. As the time axis is an indicator of the pile depth, thus the shaft resistance distribution can be interpreted from the two curves of measured force and velocity. Based on these two curves, Equation (16) was used to calculate the maximum total resistance for this pile which was 5280 kN at time t_m (which is the time of initial hammer impact) and the estimated static resistance was 2730 kN based on an assumed case damping factor J_c of 0.9 which is a typical value for firm clayey soils.

After collecting the field F and v readings, CAPWAP signal matching computer analysis was performed for this set of Fand v data to account for damping, quake, and soil static resistance variation along the pile depth. The best matched result was obtained with the following dynamic soil parameters:

- Shaft damping constant at each pile segment, J_s = 0.8 s/m
- Toe damping constant, J_t = 0.4 s/m
- Shaft quake constant at each pile segment, q_s = 2.0 mm
- Toe quake constant, q_t = 3.2 mm

The CAPWAP result for this 508-mm pile is shown in Figure 5.11. In this figure, the top-left figure shows the signal matching of computed force curve compared to the measured force curve. The top-right figure is essentially the same as Figure 5.7. The bottom-left figure was the estimated static loading performance of this pile according to shaft and toe resistance distribution. Bottom right shows the layered shaft friction distribution versus pile embedment depth, which were re-plotted and included in Figure 5.9. Figure 5.9 compares the distribution of unit shaft friction along pile length based on SPTN/WEAP and CAPWAP. There is a significant difference between two approaches, which results in a noticeable difference in predicted soil static resistances as shown in Figure 5.10.

It is noted that the final pile resistance was 2080 kN. The unit shaft friction from CAPWAP analysis was compared to static analysis (α-method) as shown in Figure 5.9. It is noted that the static analysis (α-method) overestimated and underestimated the pile shaft resistances for the shallow and deep soil deposits, respectively. Assuming a constant toe bearing resistance, the total pile resistance from CAPWAP result compared to the static analysis/WEAP is provided in Figure 5.10. As mentioned before, PDA testing and CAPWAP analysis are field direct measurement and program verification method, the estimated pile resistance is much more accurate than the WEAP bearing graph estimation which is based on general soil types and assumed dynamic soil parameters. The soil stratigraphy at the bore hole may not represent that at the test pile.

5.4 PILE RESISTANCE ASSESSMENT

As discussed above, there are two ways to assess the pile resistance:

- Given the blow count (blows / 250 mm), use WEAP bearing graph to estimate the pile resistance.
- Perform PDA testing and CAPWAP analysis to estimate the pile resistance.

It is clear to see that PDA testing would produce a more accurate estimation by collecting and analysing the field data; however, it is more expensive to conduct PDA testing which involves mounting sensors by field engineer and extra rig down time. Sometimes, re-tapping the questionable pile with specified driving energy after couple days of pile-soil setup was the preferred method for pile resistance verification. For this site, 1500 DSP were installed for the petroleum facility. Among the 800 piles, 176 piles were verified for their final pile capacity. 145 out of 176 pile resistances after setup were estimated using pile retap records and eight 508 mm piles were tested by using PDA method. Figures 5.12 to 5.15 show the estimated pile setup percentage versus dates for piles with 219-mm, 324-mm, 406-mm and 508-mm diameters. Each data point represents the estimated pile setup percentage based on the following equation:

$$Pile\ Setup\ Percentage = \frac{R_{BOR} - R_{EOID}}{R_{EOID}} \text{ x } 100\% \qquad (20)$$

where:

- R_{EOID} = estimated pile resistance at the end of initial drive, kN
- R_{BOR} = estimated pile resistance at the beginning of restrike, kN

Based on the observed setup percentage over various waiting period for those 176 piles, it is clear to see that the 82 508-mm piles were verified for setup capacities including 8 PDA tests as shown in Figure 5.14.

Based on Figures 5.12 and 5.13, it is clear to see that 219-mm and 324-mm piles have a relatively random distribution in terms of setup gain over time. The summary of 406-mm and 508-mm piles indicated a relatively consistent pile resistance increases over time. The percentages of the pile setup for all pile sizes are very similar except 219-mm piles. The reason for this is probably shorter embedment depth of 219-mm piles, and relatively weaker and more sensitive surficial soil conditions. A summary of pile setup gain observed from pile installations and re-tap is provided in Table 5.2. The variation in pile embedment depth does not really affect the setup percentage. The estimated pile setup gain percentage will be compared to the numerical analysis results in Section 6.0.

Table 5.1. Recommended Quake and Damping Parameters in WEAP

Soil Type	Shaft Quake (mm)	Toe Quake (mm)	Shaft Damping (s/m)	Toe Damping (s/m)
Cohesive	2.0 – 3.5	Pile Diameter / 60	0.7 – 1.3	0.5 – 0.6
Non-cohesive	1.5 – 3.0	Pile Diameter / 120	0.6 – 0.9	0.3 – 0.5
Bedrock	1.0 – 2.0	2.5	0.5 – 0.8	0.1 – 0.3

Table 5.2. Summary of Observed Pile Setup

Pile Diameter (mm)	No. of Piles Studied	Pile Embedment Depth (m)	Setup Percentage (%)	Pile Resistance Increase (kN)
219	30	12 - 16	14 - 155	140 - 595
324	45	12 - 20	15 - 132	180 - 950
406	17	12 - 20	47 - 138	394 – 1158
508	84	16 - 20	10 - 138	730 - 1550

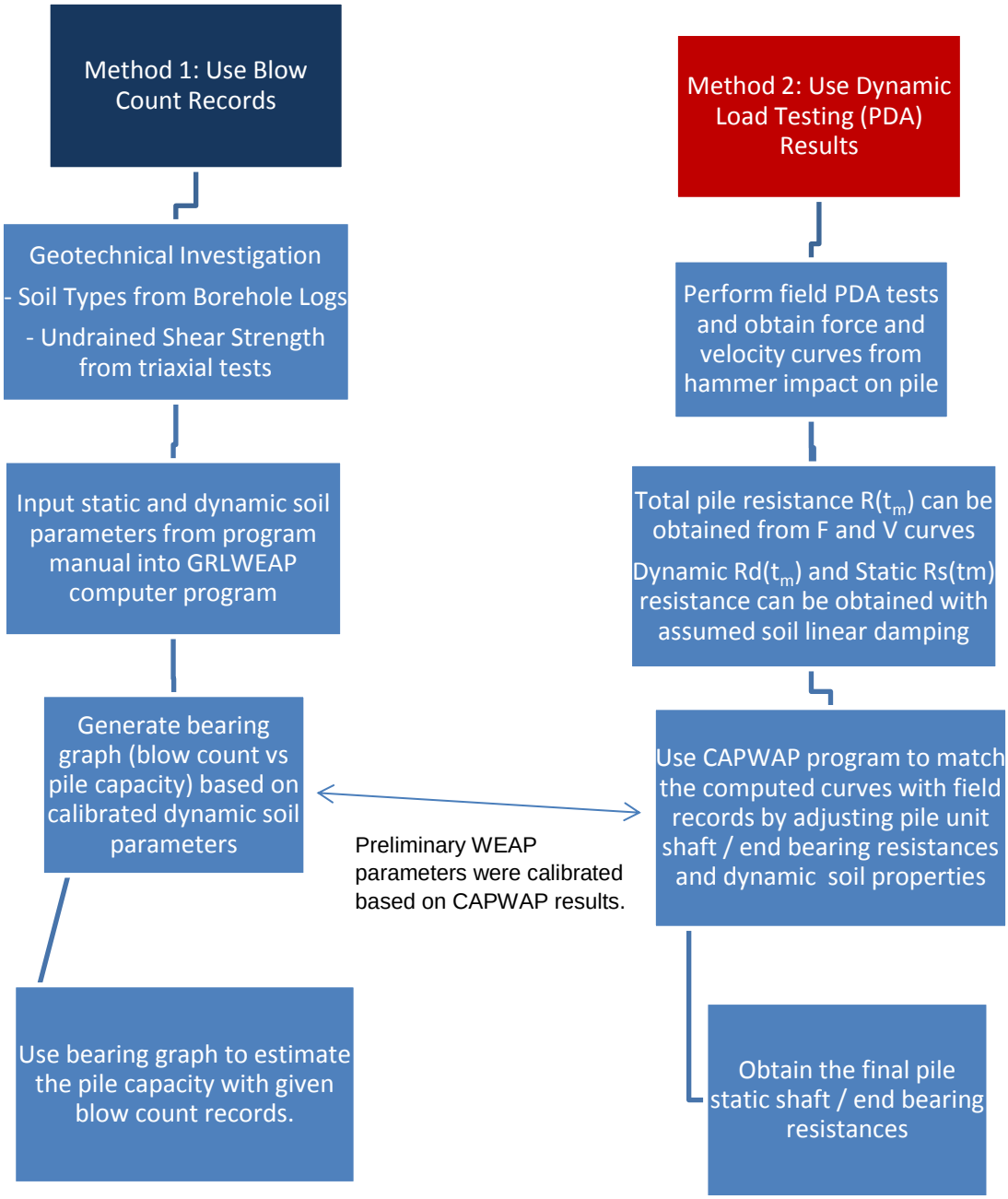

Figure 5.1. Flow Chart of Pile Setup Estimation

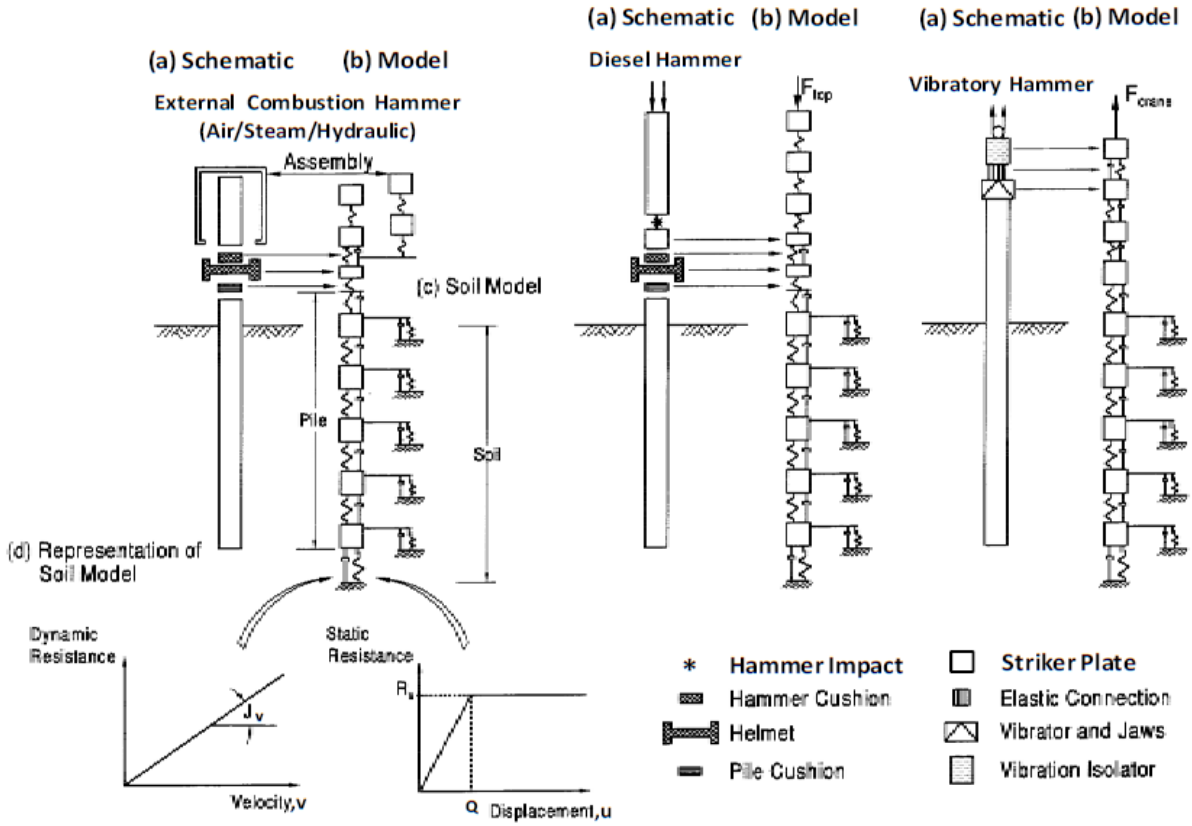

Figure 5.2. Wave Equation Models for Multiple Hammer Types (Hannigan, 1998)

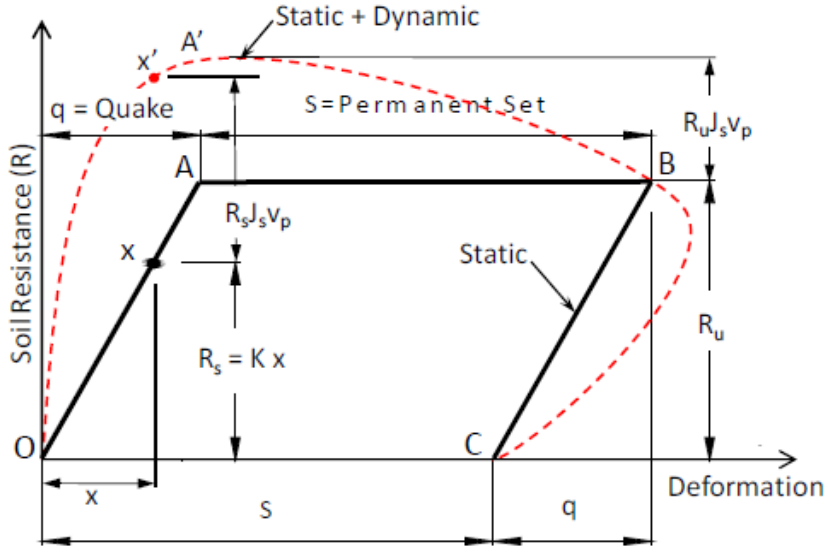

Figure 5.3. Stress Strain Diagram of the Soil Resistance at a Pile Point (Smith, 1960)

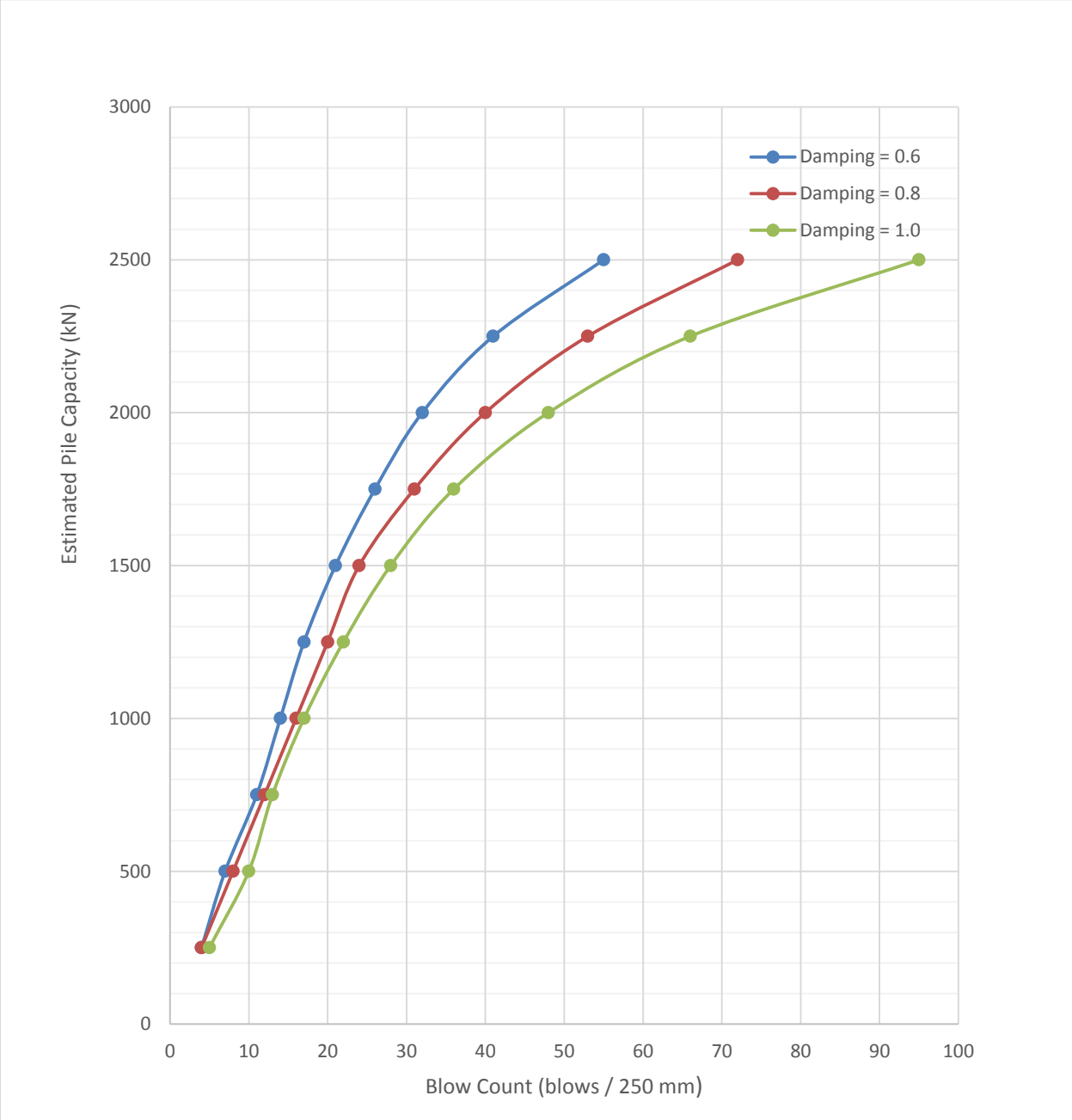

Figure 5.4. Bearing Graph of a Pile at the Design Depth

Figure 5.5. PDA Sensors Mounting Diagram (ParklandGEO, 2018)

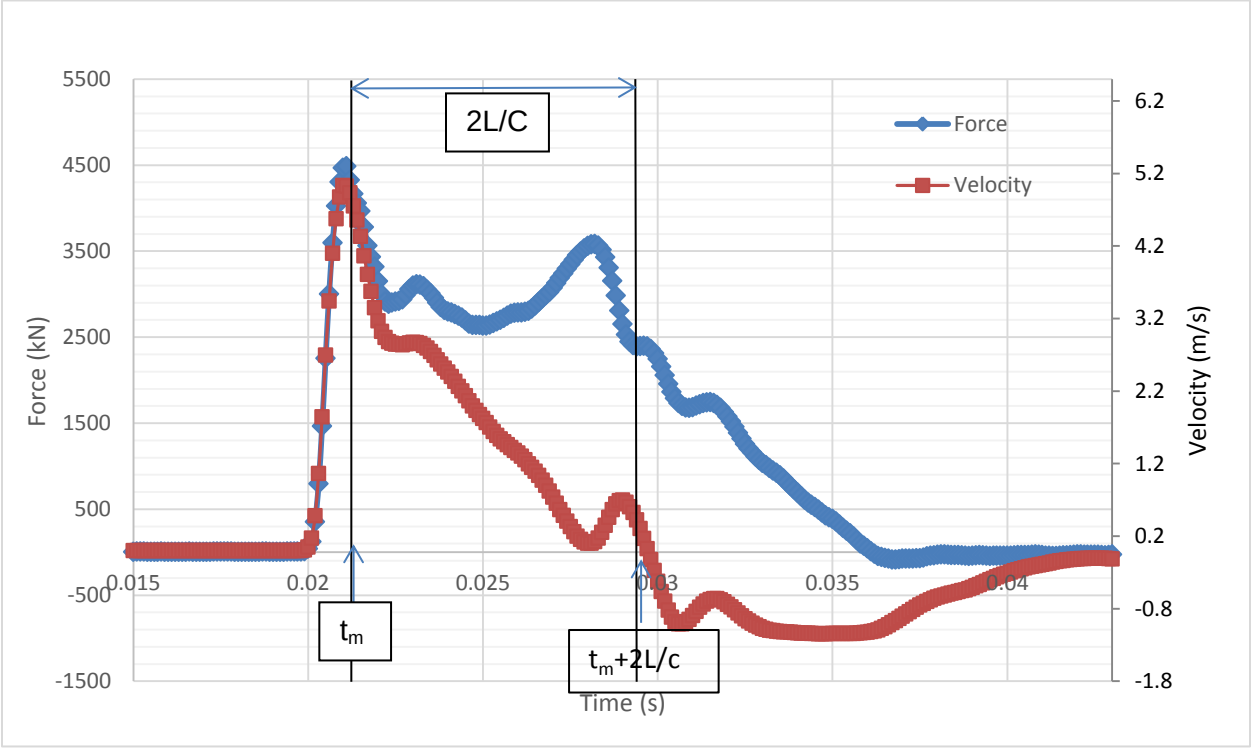

Figure 5.6. Force and Velocity Measurements from a Hammer Blow

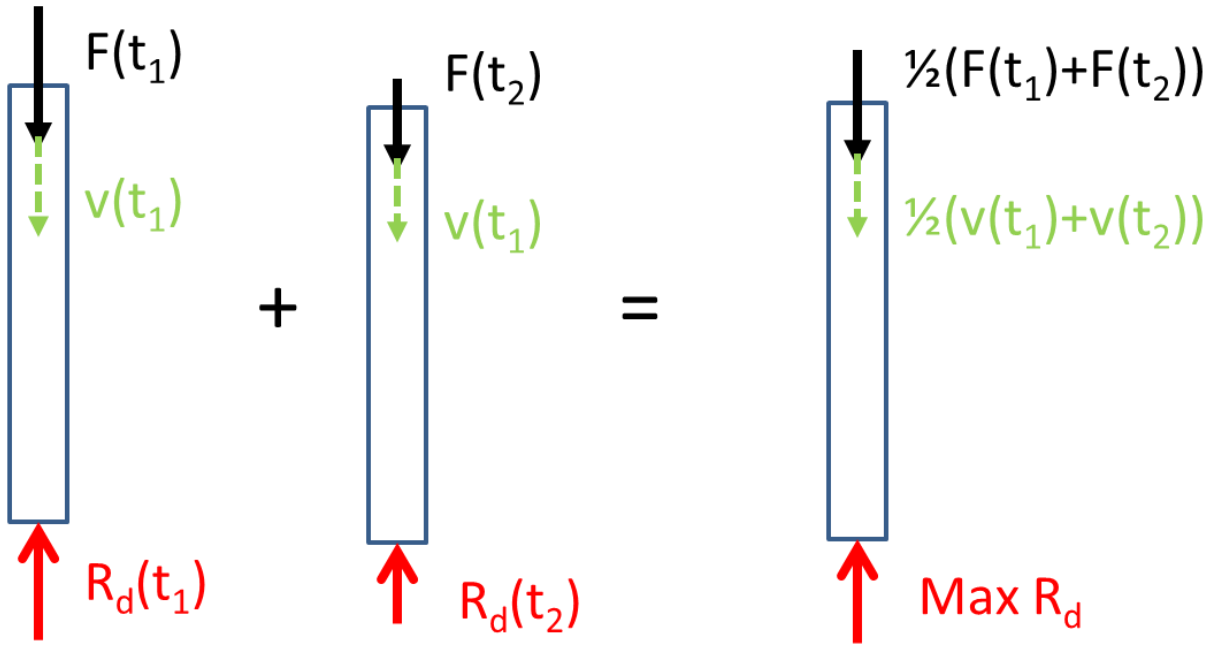

Figure 5.7. Case Method – Relationship among Measured Forces, Velocities at Pile Top and Soil Resistance

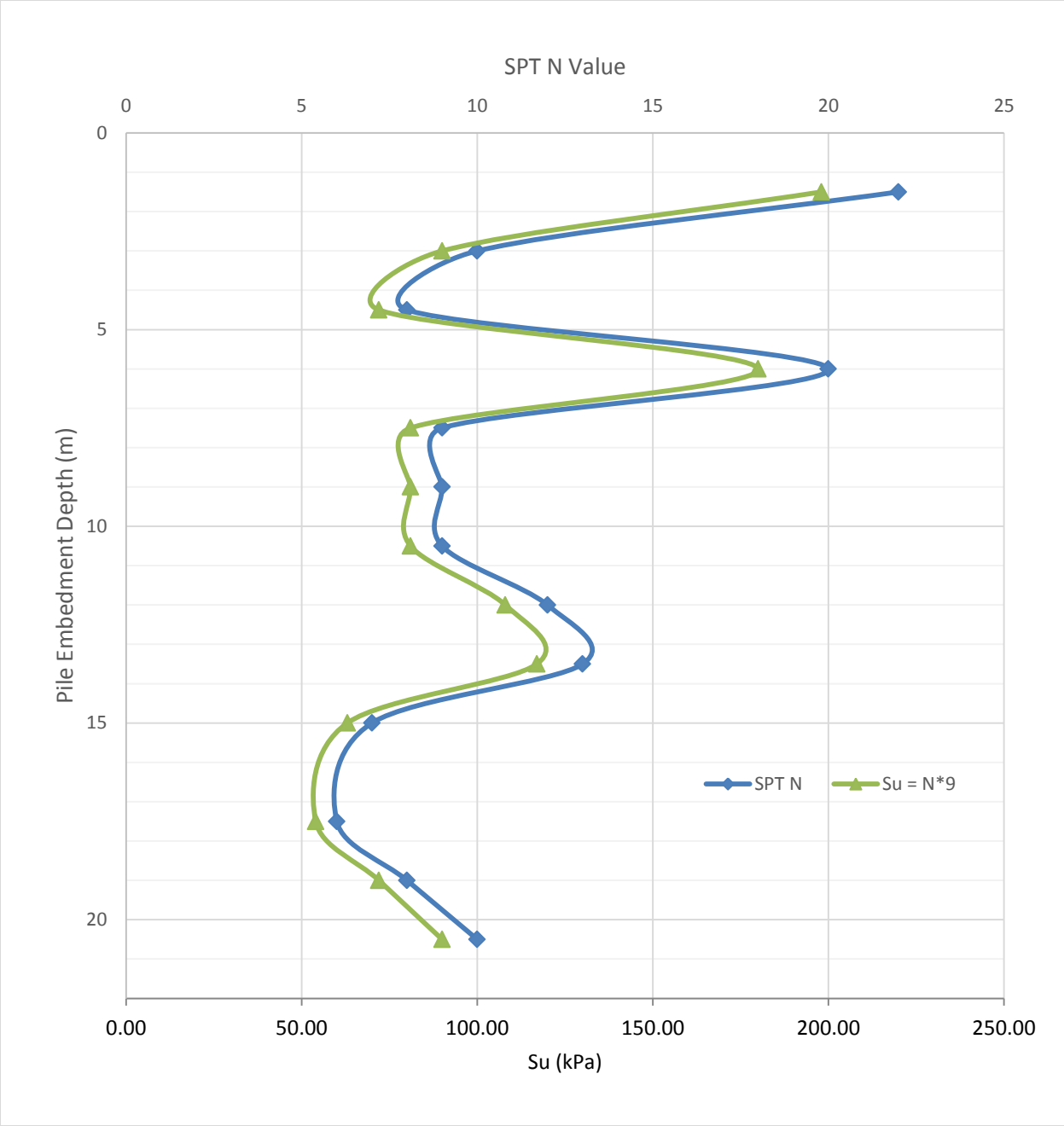

Figure 5.8. SPTN and Undrained Shear Strength (S_u) of Clay

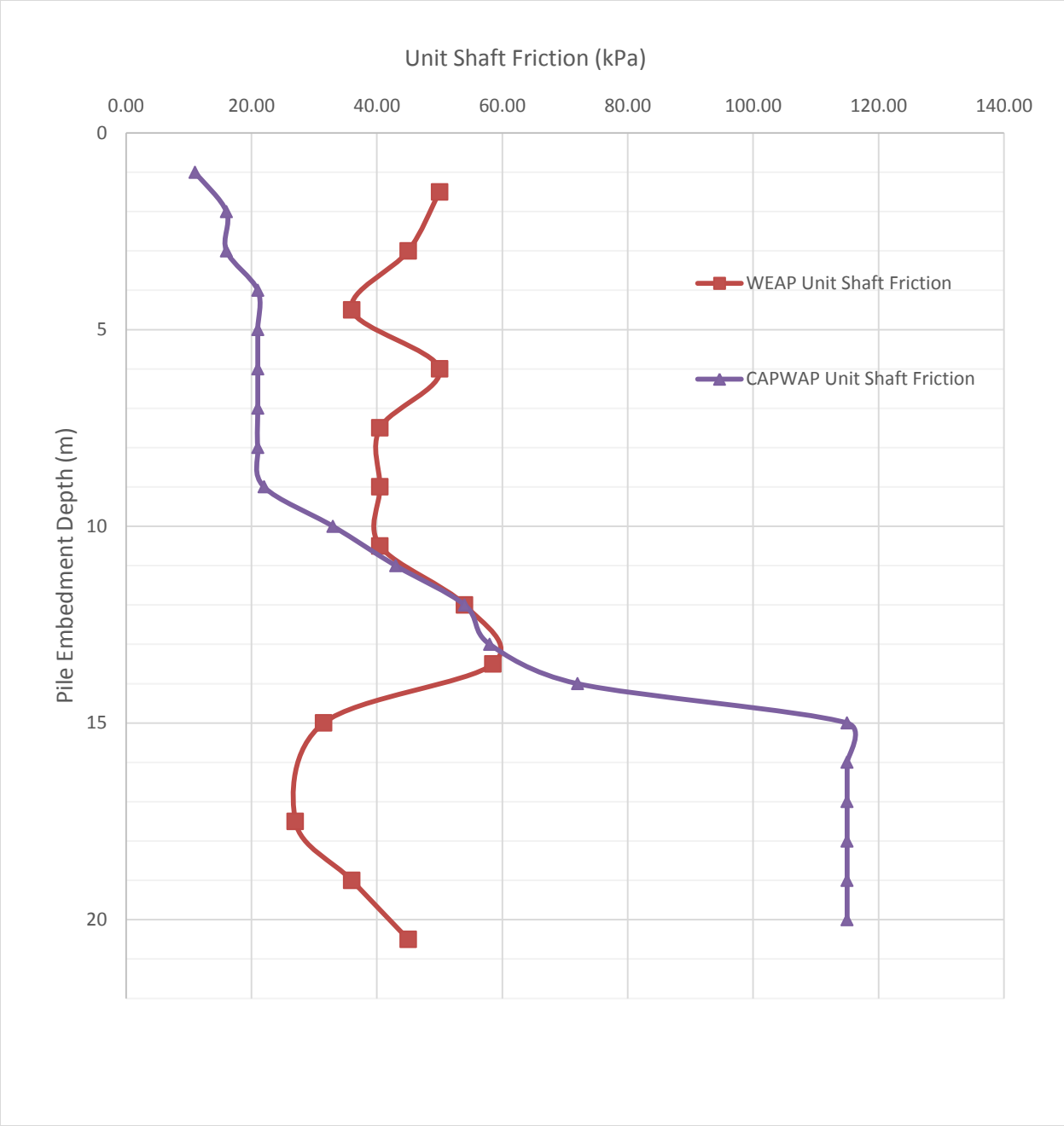

Figure 5.9. Unit Shaft Friction From WEAP and CAPWAP

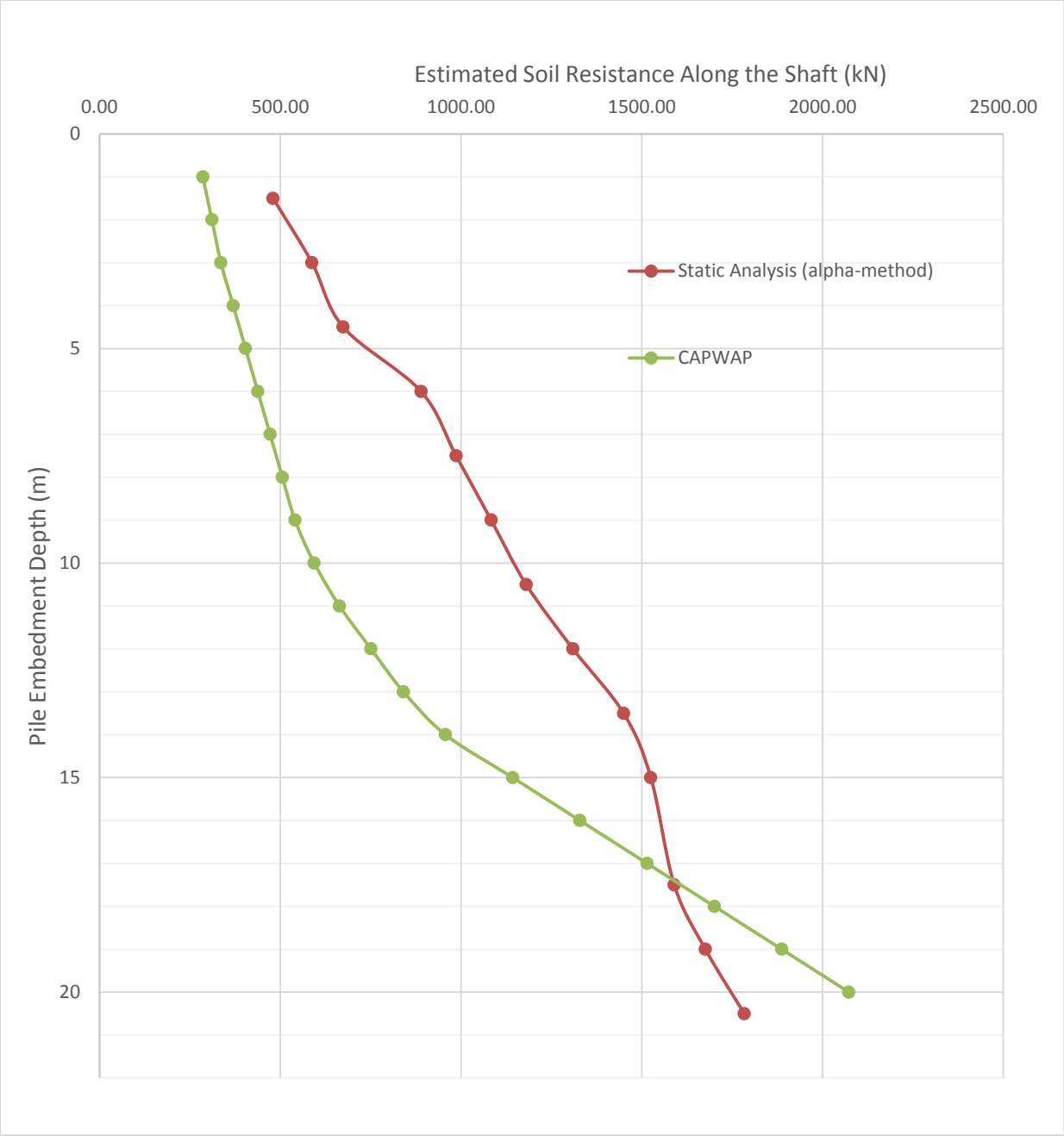

Figure 5.10. Estimated Pile Resistance by Static Analysis versus PDA/CAPWAP at 20 m

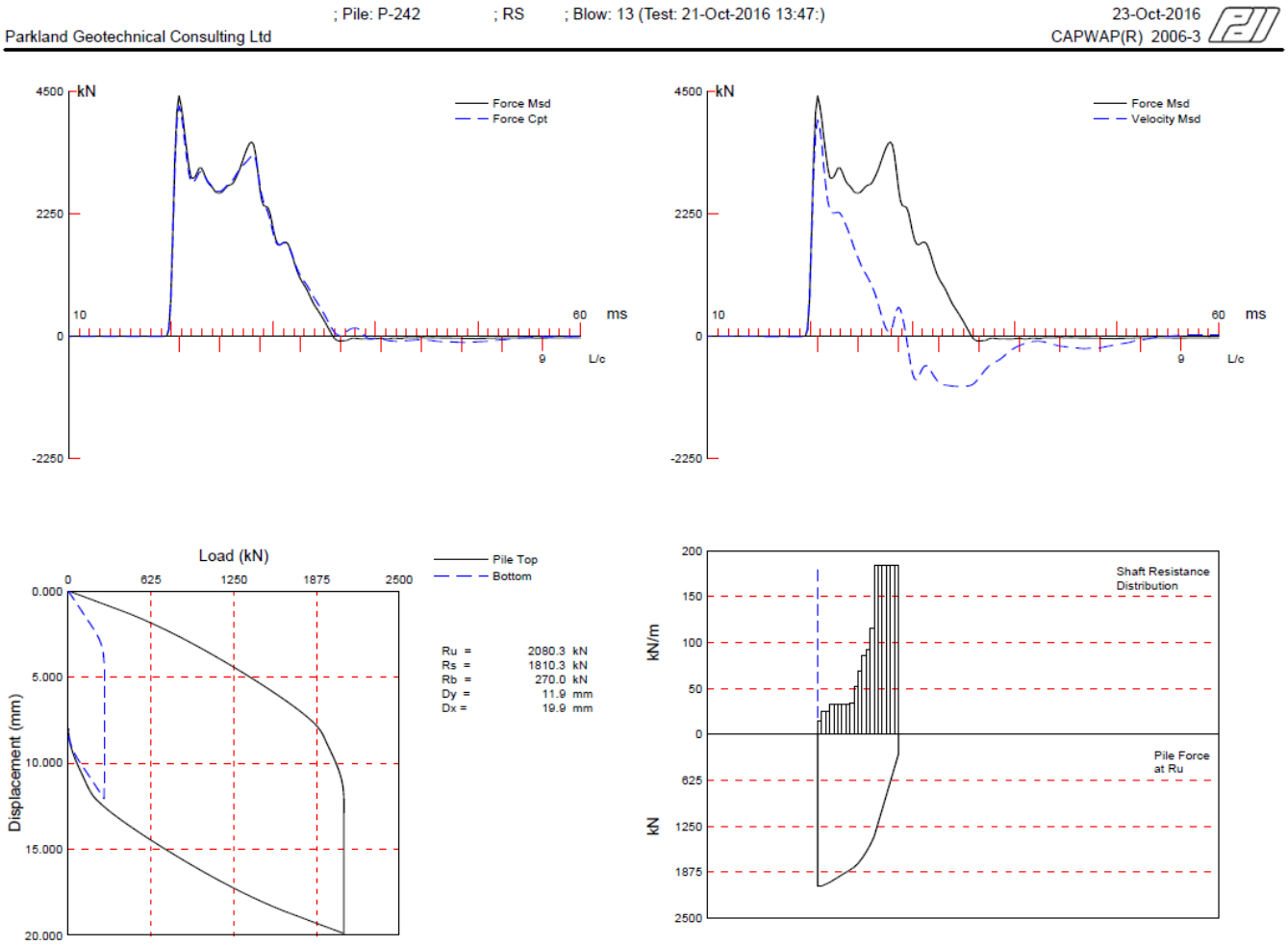

Figure 5.11. CAPWAP Output Sample (ParklandGEO, 2018)

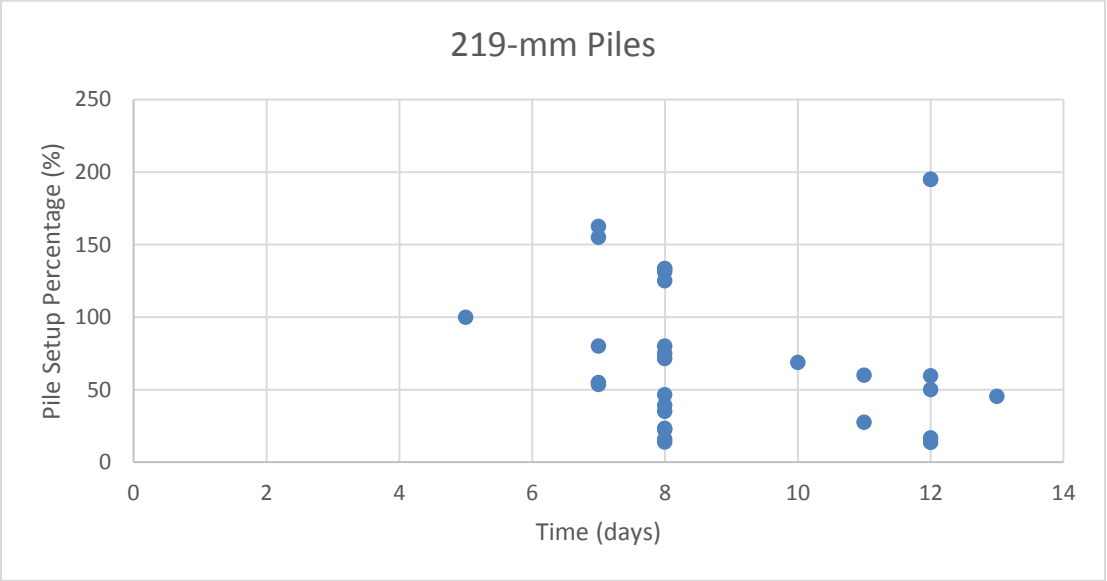

Figure 5.12. Pile Setup Percentage for 219-mm Diameter Piles

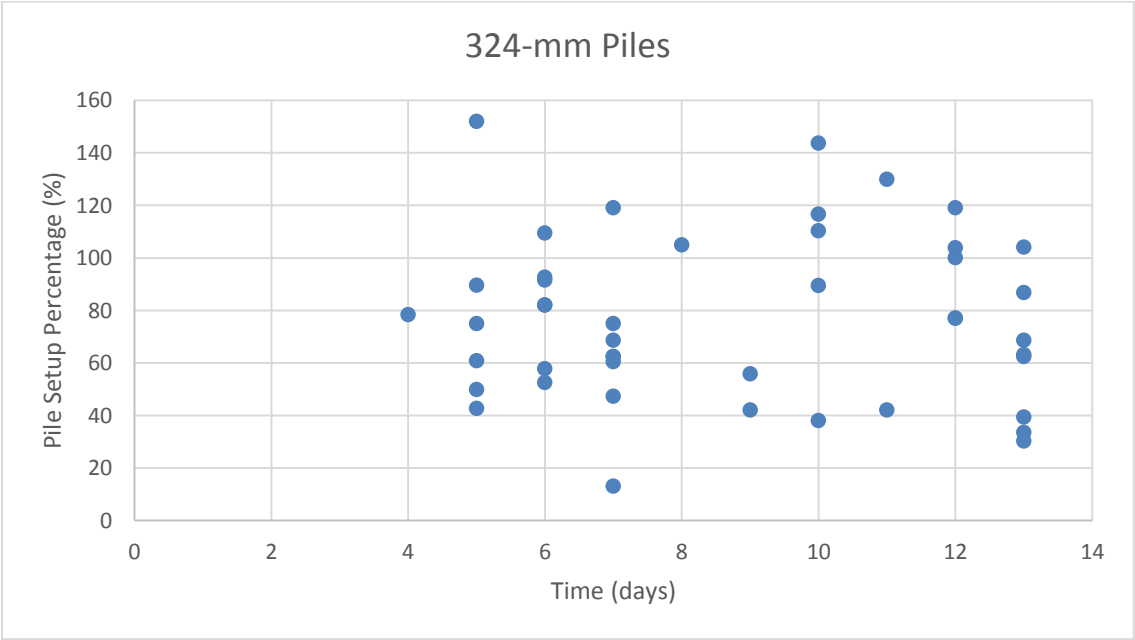

Figure 5.13. Pile Setup Percentage for 324-mm Diameter Piles

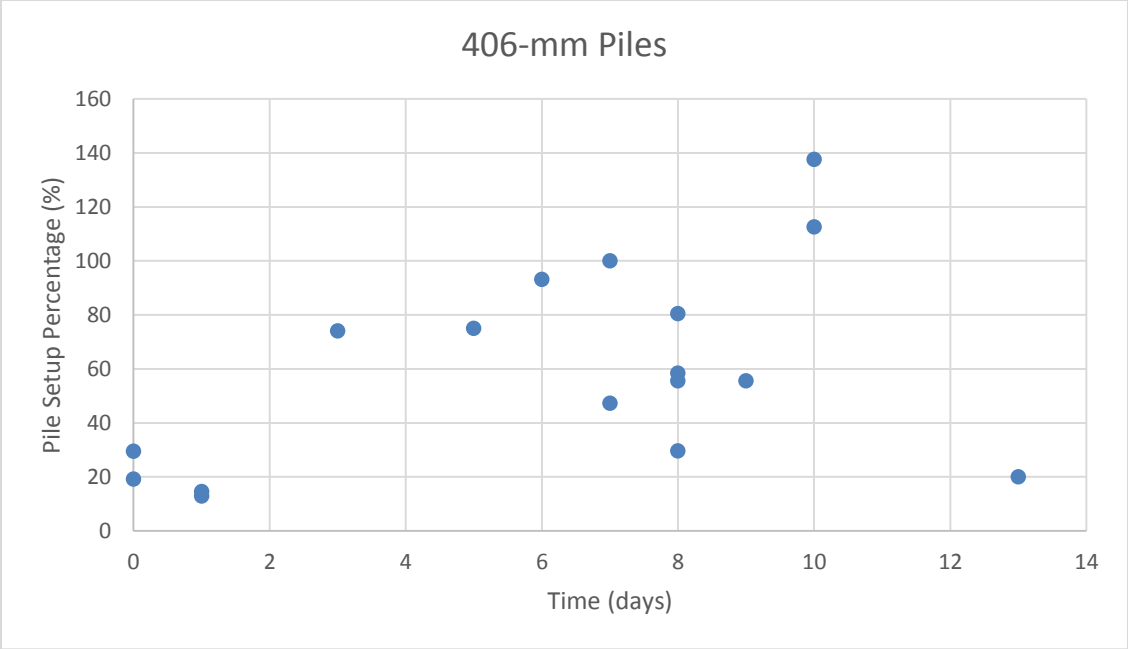

Figure 5.14. Pile Setup Percentage for 406-mm Diameter Piles

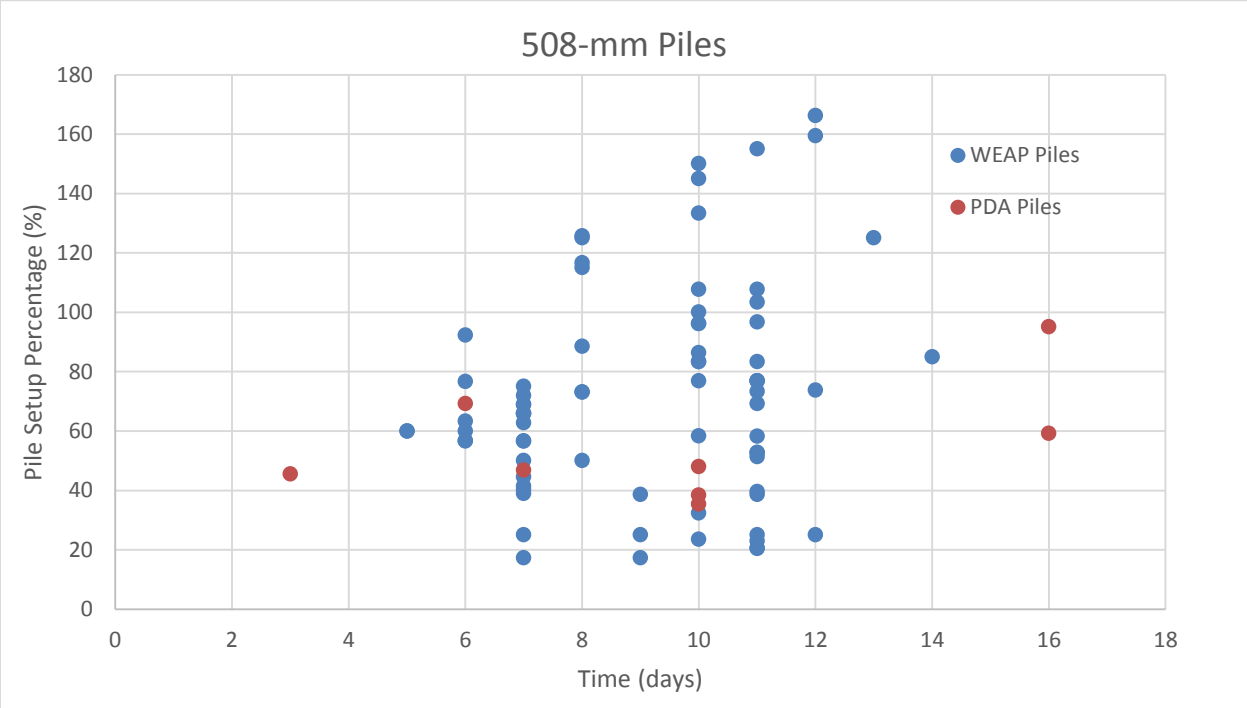

Figure 5.15. Pile Setup Percentage for 508-mm Diameter Piles

6.0 FINITE ELEMENT MODELING OF PWP DISSIPATION

6.1 CRYER EFFECT

ABAQUS was used for the finite element modelling (FEM) of pore water pressure dissipation and pile-soil setup. In this section, Mandel-Cryer Effect was modelled to verify if ABAQUS FEM model performs as expected.

Generally, the Mandel-Cryer Effect describes the saturated porous material subject to surcharge load and subsequent pore pressure dissipation behaviour (Mandel, 1953) and (Cryer, 1963). Because the Mandel-Cryer porous material consists of a spherical shape, this pore pressure dissipation effect is considered as a 3-D consolidation. Parameters used in this FEM model are provided in Table 6.1. The poisson ratio of 0.33 was selected as per research paper prepared by Wong (1998). Due to the relative small size of this model, a quite low permeability was selected to extend the pore pressure dissipation period to about 300 days.

The Mandel-Cryer Effect modelled by ABAQUS is provided in Figures 6.1 and 6.2. Figure 6.3 provides the initial pore water pressure increase and dissipation over 500 days. It is noted that the modelled results met the expectation of pore water pressure dissipation during 3-D consolidation.

6.2 NUMERICAL MODELLING OF PILE SETUP

6.2.1 Model Assumptions, Input and Soil Parameters

Based on information and figures provided in Section 5.4, piles with 508-mm diameter had the most field data and relatively similar embedment depths. Also, piles with this large diameter installed in the soft to firm clayey soil are less likely to plug during the installation. This is because larger pile needs more internal skin friction to form a solid plug. Therefore, in this numerical modelling, 508-mm piles were modelled. The assumptions of this ABAQUS model are provided below:

- It is assumed that the 508-mm piles are not fully plugged during the installation, so the induced soil displacement due to pile driving will be the steel pipe thickness which is 12.7 mm. A cavity expansion was conducted in the ABAQUS for this soil displacement.
- Given the induced displacement of 12.7 mm which is about 5% of strain considering the radius of the pile is 508 mm. It is assumed this deformation of the clayey soil is still within the elastic region.
- In the field, it is common to see ponding water around the pile perimeter, therefore, this model assumed that the excess pore pressure would dissipate through the shear zone between the pile shaft and soil interface.

Detailed soil parameters are provided in Table 6.2.

6.2.2 Element Type and Boundary Conditions

An 8-nodes axisymmetric quadrilateral, biquadratic displacement, bilinear pore pressure, reduced integration (CAX8RP) element type was selected for this model. The main reason of this element type selection is because it generates expected output under reasonable computing time (about 300 seconds). A total of 338 elements and 341 nodes were included in this model. The applied boundary conditions and simulation steps are provided as follows:

- BC-1: Fixed displacement at X and Y directions for the bottom and right sides at initial step.
- BC-2: Fixed displacement at X and Y directions for the left side below the pile toe at initial step.
- BC-3: Applied 10 / 20 mm of displacement along the cavity in radial direction at Step 1.
- BC-4: Zero pressure along the pile shaft area at Step 2.
- Allow pore water pressure dissipation in Step 2 for up to 100 days after the induced displacement in Step 1.

A schematic diagram of the above boundary conditions is provided in Figure 6.4. The length of the cavity expansion is about 20 m deep. The in-situ pore water pressure, model dimensions and mesh are shown in Figure 6.5.

6.3 NUMERICAL MODELLING RESULTS AND COMPARISON

Pore Pressure Dissipation along the Pile Shaft

After constructed the cavity expansion modelling in ABAQUS, numerical analysis has been conducted for the pore water pressure dissipation simulation subsequent to the pile installations. The PWP during the pile driving is shown in Figure 6.6. The PWP dissipation at the mid-point of the pile shaft (about 11 m below ground) is shown in Figure 6.7. Horizontal effective stresses were also obtained from this numerical model. In order to compare the pore water pressures, radial effective stresses along the pile shaft and away from the pile location, the results have been processed to be dimensionless by dividing radial distance L by pile radius r. A permeability of $2.3*10^{-10}$ cm/s was used in this analysis and the results are shown in Figure 6.8.

As per Figure 6.8, the radial effective stress increase along the depth of the pile shaft was relatively uniform. This is due to the assumed constant soil stiffness, void ratio and Poisson's ratio over depth in the ABAQUS model.

Based on the geotechnical report, the clay and clay till deposits are quite similar and consistent over the depth. Therefore, it is acceptable to study a certain depth along the pile shaft. The depth selected was the middle point which was about 11 m below grade.

Pore Pressure Dissipation in Radial Direction

As mentioned above, elements at about 11 m below grade were studied to see the pore pressure influence zone in radial direction. Figures 6.9 and 6.10 provide the pore water pressure dissipation and radial effective stress increase versus the radial distance from the pile location.

Based on the above figures, we can see that pore water pressure effect zone was about 27 times radius of the pile. For this 508-mm diameter pile, the pore pressure effect zone was 6.8 m. It also appears that 90% of the pore water pressure dissipated over the first 30 days for a permeability coefficient of $2.3*10^{-10}$ cm/s. With a decreased permeability coefficient, the required time to achieve a minimum of 90% of pore water pressure will increase.

Induced Displacement Effect

The induced displacement effect is also studied based on two displacements of 10 mm and 20 mm to allow possible pile wall thickness variation (eg. steel pipe welding joint), and the PWP response is provided in Figure 6.11.

Based on Figure 6.11, the induced excessive pore water pressure due to 20 mm displacement was about 15% and 10% higher than the 10 mm case at day 0.1 and day 100, respectively. The dissipation behavior from both displacement cases was relatively similar. Double the amount of strain in this model only causes about 10% to 15% of pore pressure change. Therefore, the variation in induced displacement is not considered as a critical parameter.

Comparison between Field Data and FEM Results

After studied all the relevant parameters included in this numerical model, the comparison between the field observation data and numerical analysis results have been undertaken.

Figure 6.12 provides the comparison between the estimated setup percentage and capacity gain from both field observation and numerical modeling for 508-mm diameter piles.

Based on Figure 6.12, the setup percentage of field observation deviated more from the numerical simulation. It is probably caused by the initial pile capacities were being under estimated due to extremely low blow count readings (3 to 8 blows / 250 mm) which cannot be property estimated based on WEAP bearing graph.

In terms of the optimized pile final capacity verification period, 10 to 20 days will be the most ideal time frame. This time is highly sensitive to the permeability of the soil deposits. In sandy soil, the verification time can be reduced to 1 to 3 days. Silty soil would need about 7 days and high clay content soil may need up to 20 days of setup time.

Table 6.1. Soil Parameters for Cryer Effect Model

Diameter (m)	Elastic Modulus (Pa)	Poisson's Ratio	Void Ratio	Permeability K (cm/s)
0.25	$1x10^{7}$	0.33	0.4	$1.7x10^{-12}$

Table 6.2. Soil Parameters for Cavity Expansion Model

Radius of Cavity (m)	Elastic Modulus (Pa)	Poisson's Ratio	Void Ratio	Permeability K (cm/s)
0.25	$1x10^{7}$	0.35	0.4	$2x10^{-9}$ to $2x10^{-10}$

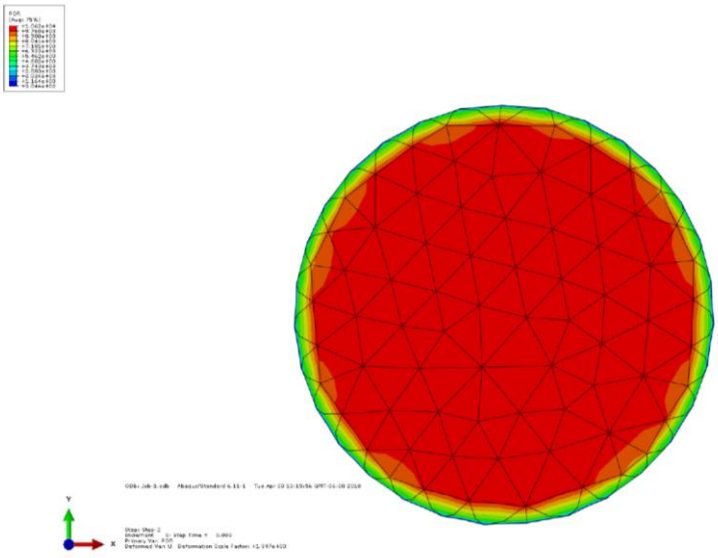

Figure 6.1. Pore Water Pressure After Applying a Surchage of 10 kPa

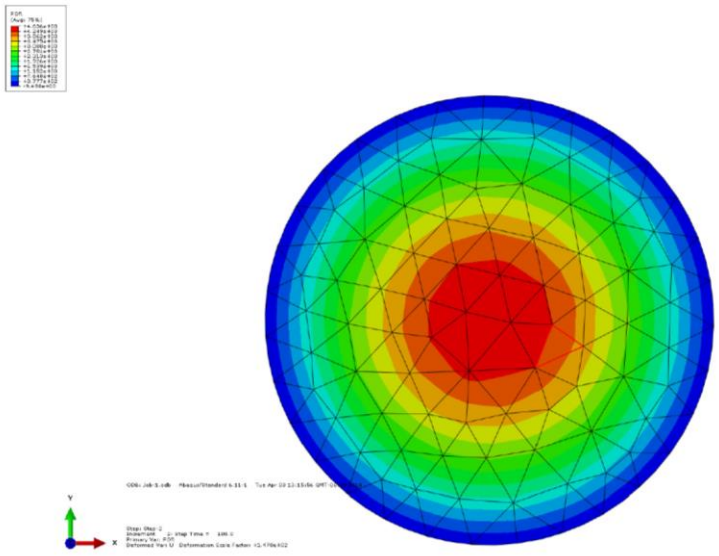

Figure 6.2. Pore Water Pressure After 1000 Days of Dissipation

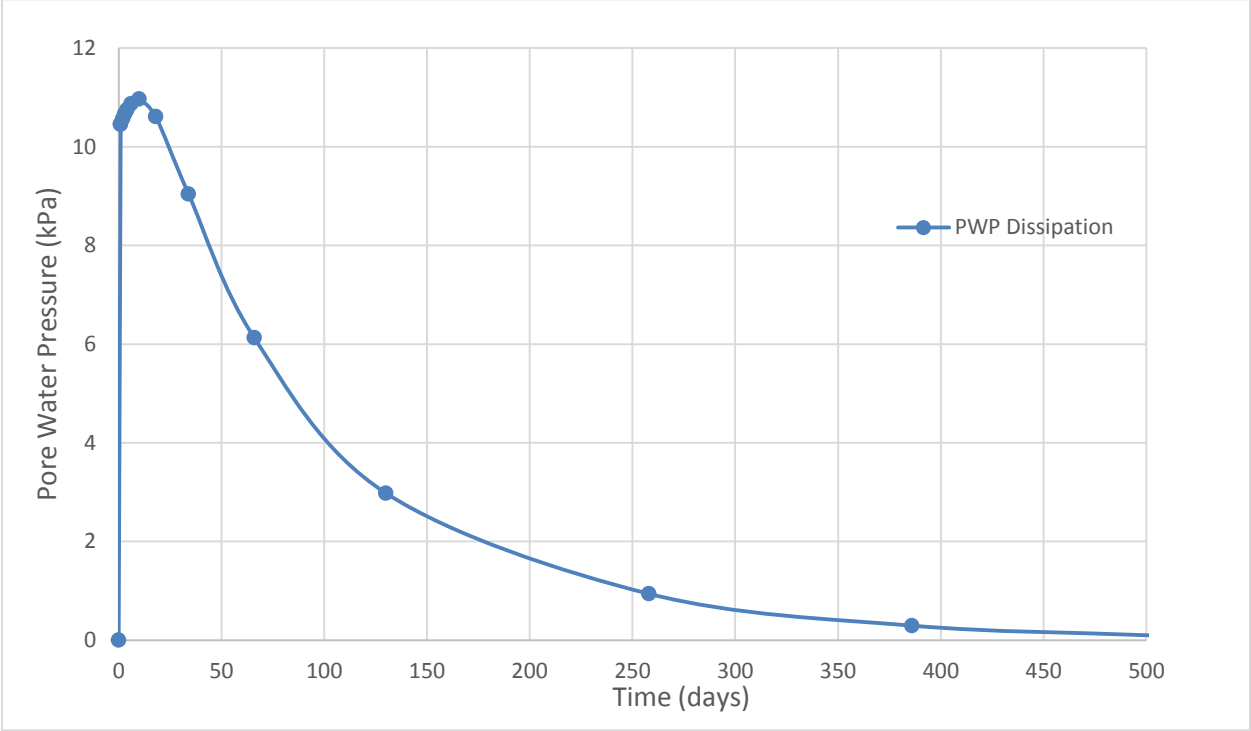

Figure 6.3. Pore Water Pressure Dissipation vs Time

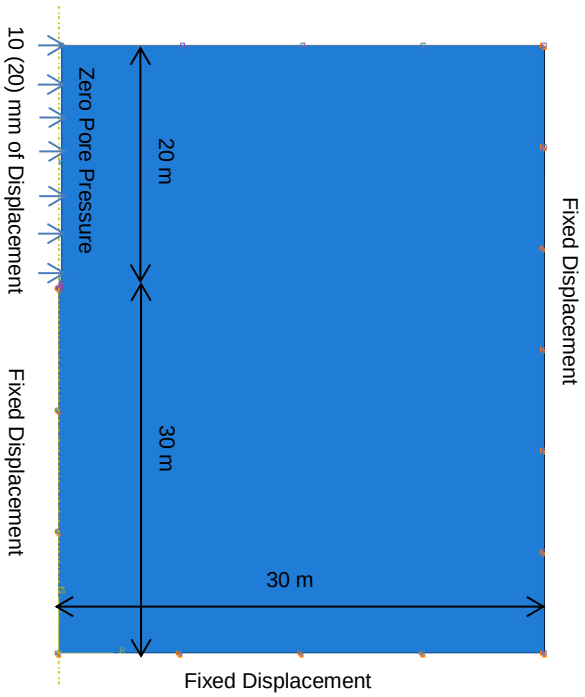

Figure 6.4. Schematic Diagram of Boundary Conditions for Cavity Expansion Model

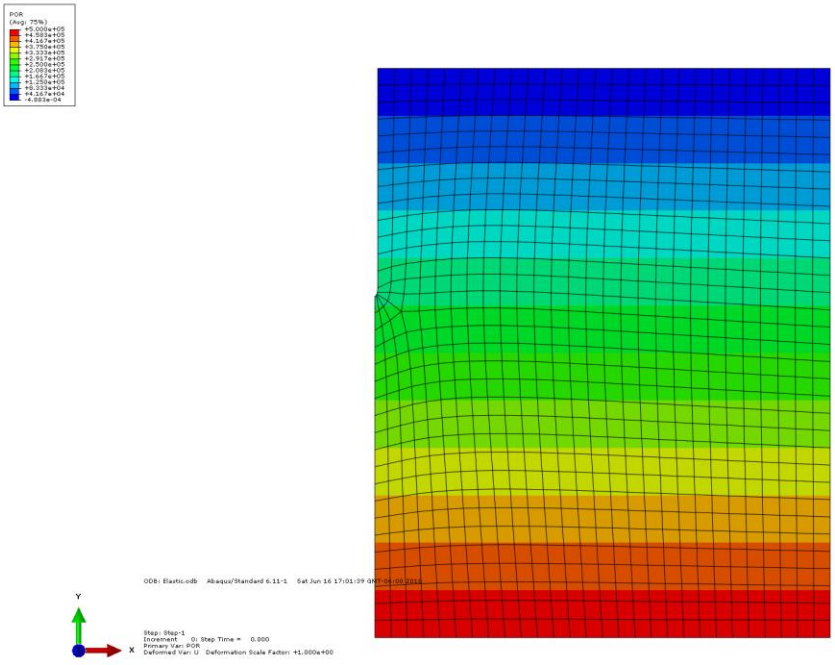

Figure 6.5. In-situ Pore Water Pressure Distribution Prior to Cavity Expansion

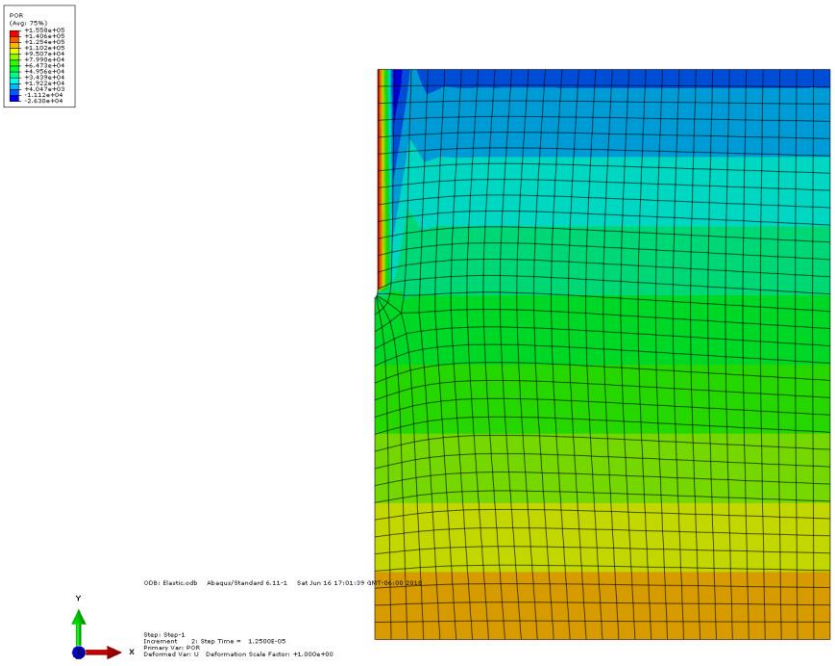

Figure 6.6. Pore Water Pressure During Cavity Expansion At t = 0.01 hr

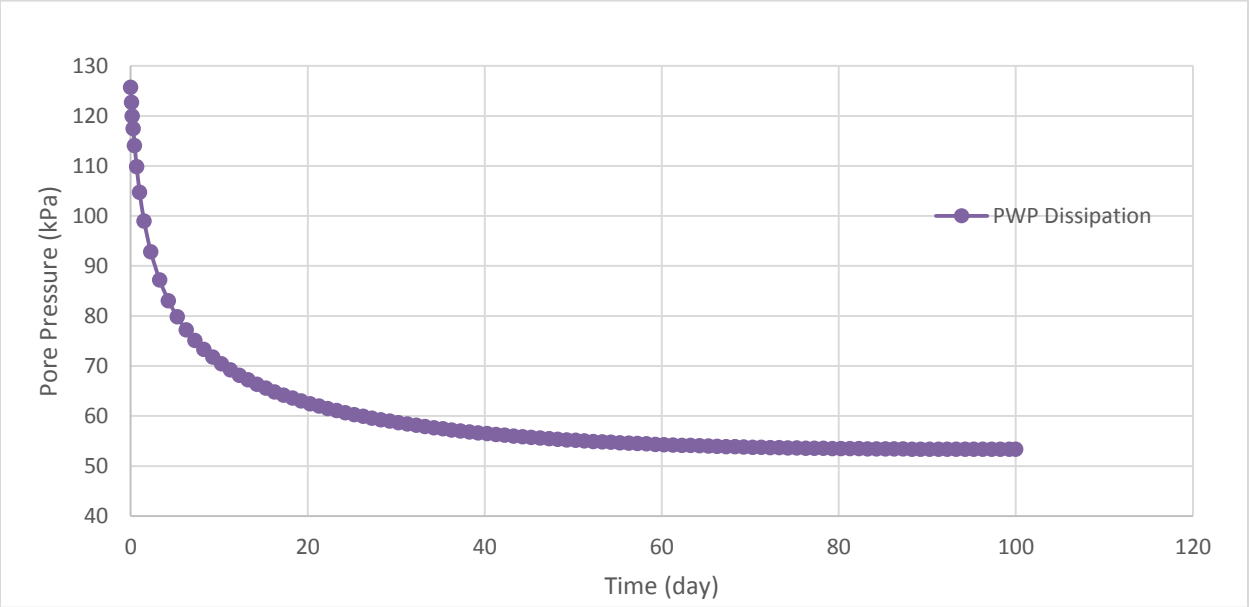

Figure 6.7. PWP Pressure Dissipation at Depth of 11 m (k=2e-10 cm/s)

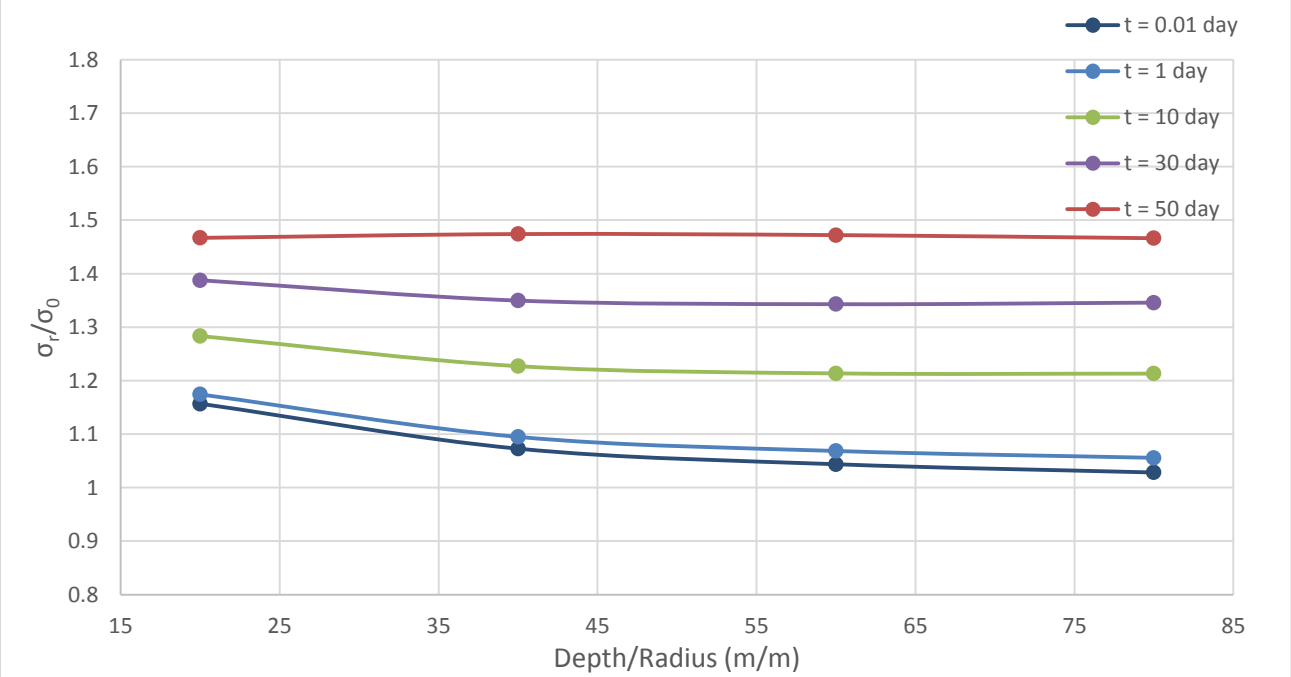

Figure 6.8. Radial Effective Stress vs Pile Depth Along Shaft (k=2e-10 cm/s)

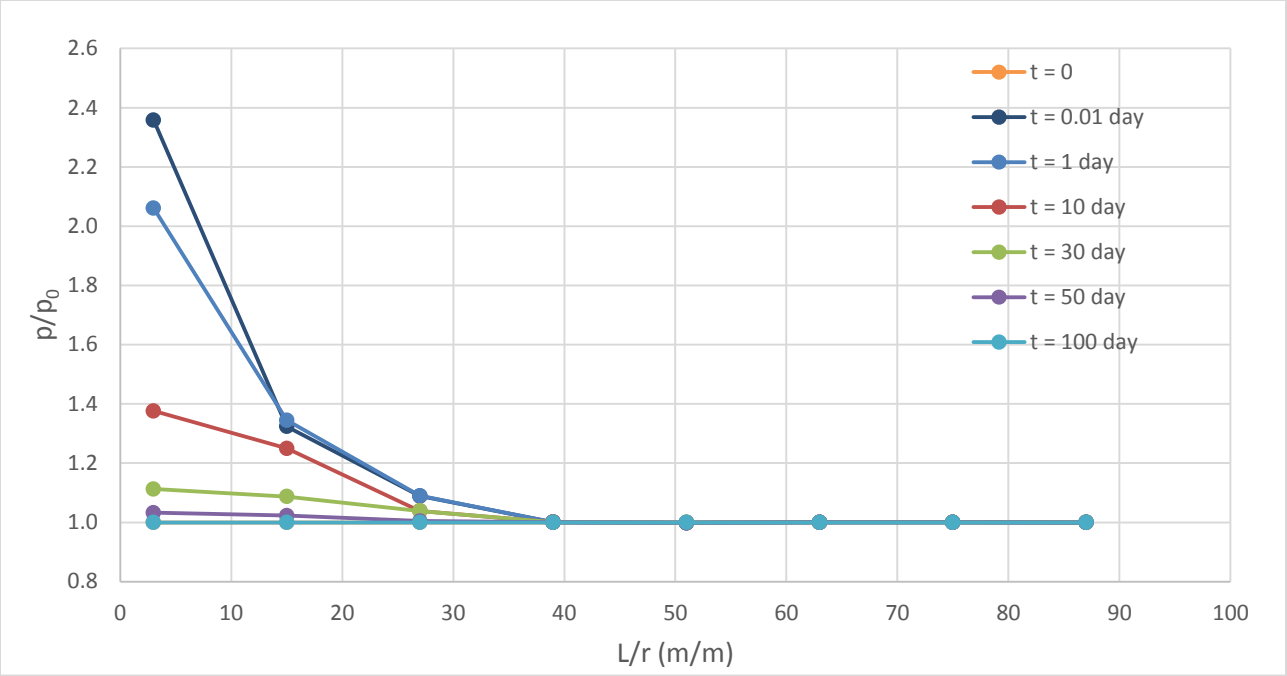

Figure 6.9. Pore Water Dissipation vs Radial Distance from Pile Location at Depth of 11 m (k=2e-10 cm/s)

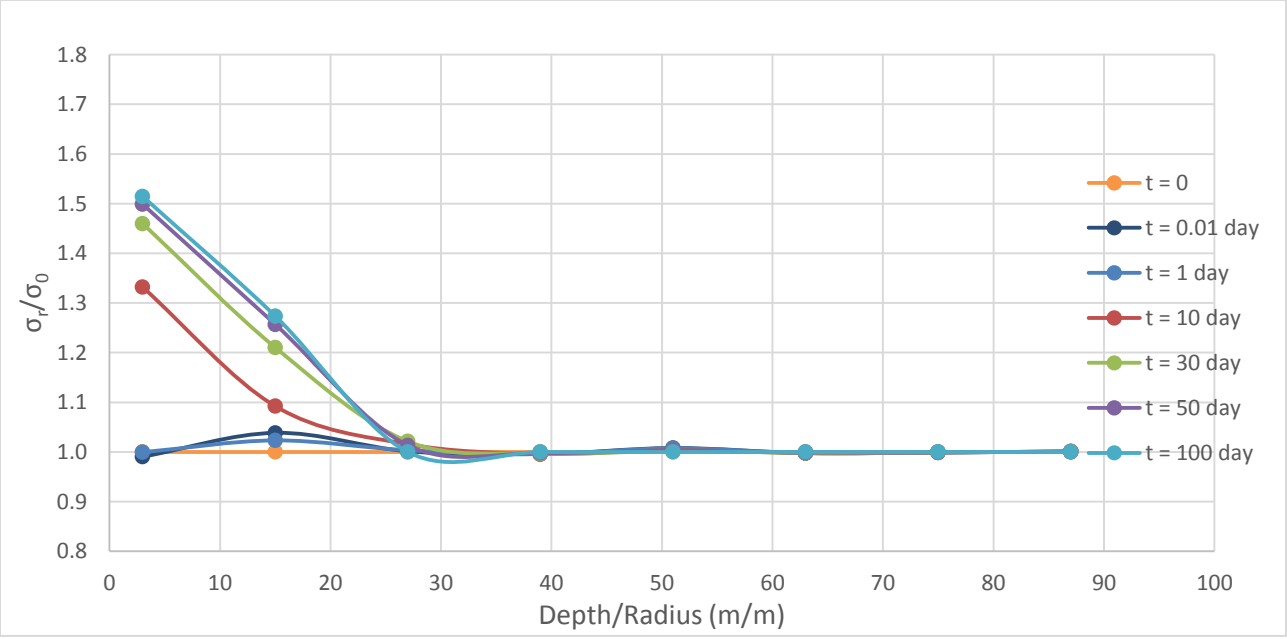

Figure 6.10. Radial Effective Stress vs Radial Distance from Pile Location at Depth of 11 m (k=2e-10 cm/s)

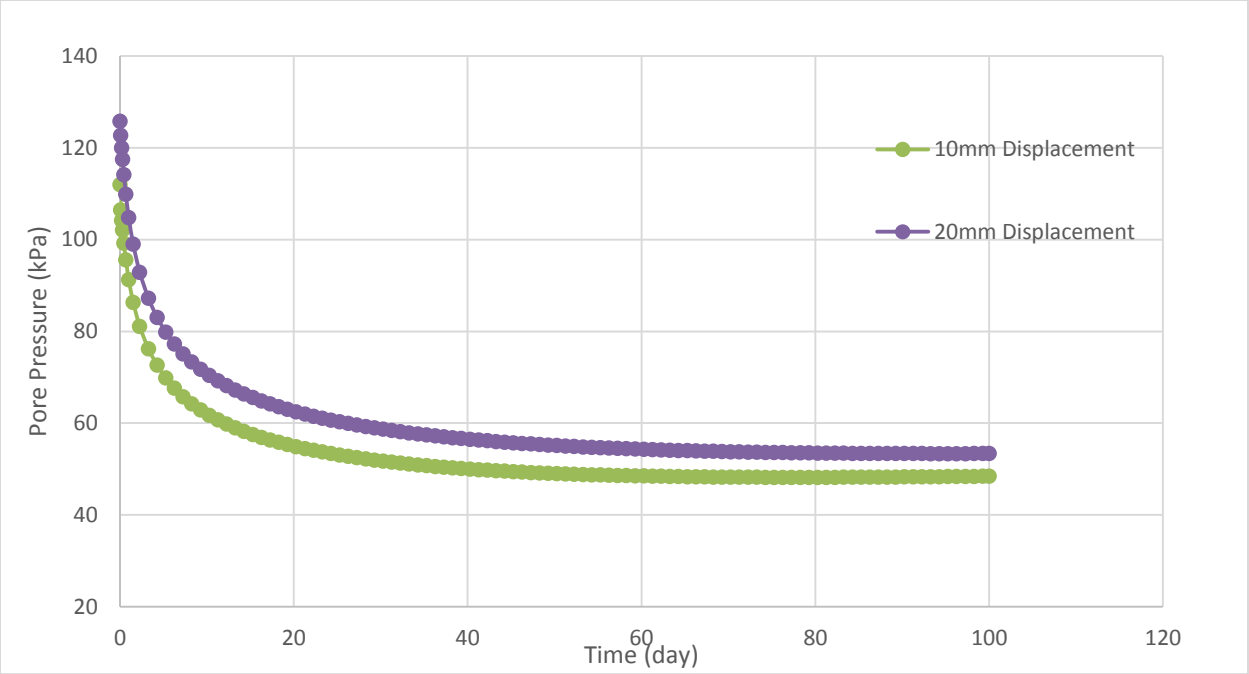

Figure 6.11. Pore Water Dissipation with Different Induced Displacements

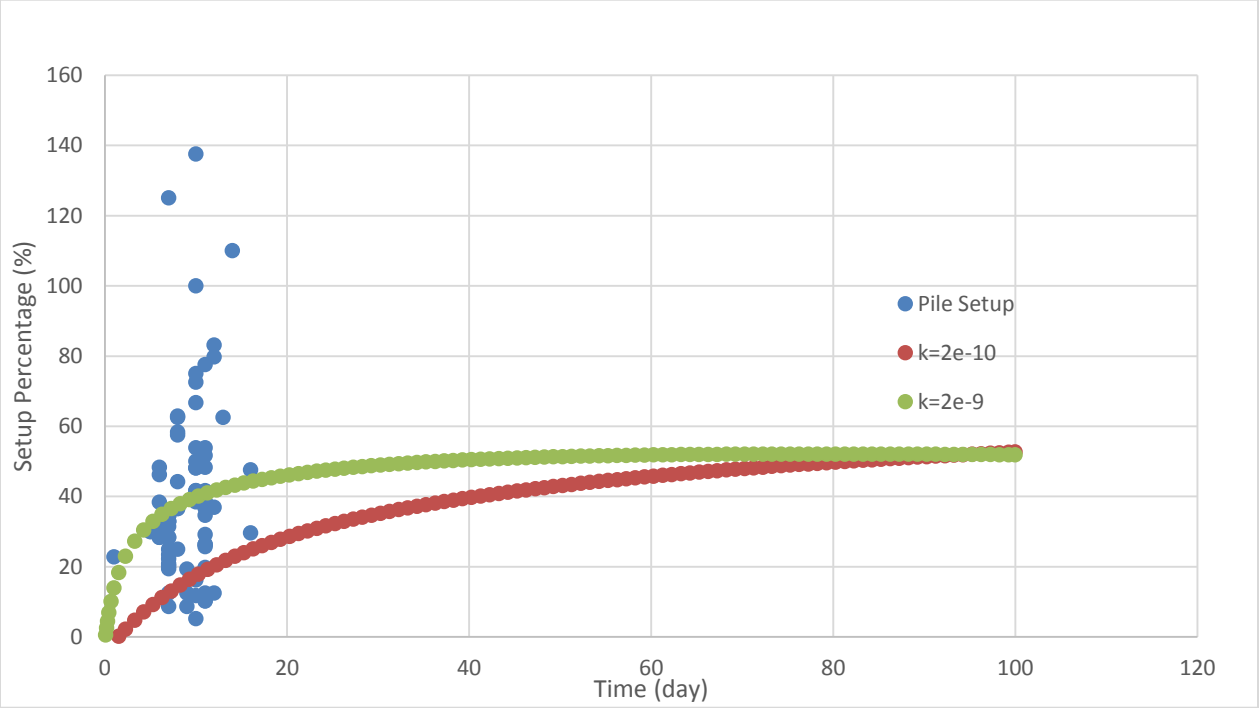

Figure 6.12. Pile Setup Percentage vs Time

7.0 SUMMARY

In summary, the pile setup effect in clayey soils deposits near Edmonton area were studied by using FEM method. The key assumption in this FEM model was that pore water pressure dissipation following the initial pile installation was the major source of pile capacity setup behavior. A summary of field observation has been provided for different pile sizes installed at the site. Numerical modeling by ABAQUS was undertaken to study the parameters and simulate the field observation of pile setup.

In this study, only elastic model was used in this FEM model provided with un-plugged pile condition. For pile with diameter smaller than 324 mm (12"), it is more likely the pile toe will be plugged during driving and the induced soil displacement will be significantly larger than the assumption made in this study. Further plastic deformation model will be required to simulate the plugged condition.

Overall, the FEM method is a power tool to estimate the setup time required to reach 90% of PWP dissipation for the piles found in different soil deposits as shown in Figure 6.12. It could be used to provide an optimum pile re-tap or PDA restrike testing time frame in order to reduce the waiting or down time during the foundation constructions.

8.0 REFERENCES

Andriashek, L. (1988). *Quaternary Stratigraphy of the Edmonton Map Area.* Terrain Sciences Department, Natural Resources Division Alberta Research Council, Open File Report #198804.

ASTM D4945-17. (2017). *Standard Test Method for High-Strain Dynamic Testing of Deep Foundations.* West Conshohocken, PA: ASTM.

Biot, M. A. (1941). General Theory of Three-Dimensional Consolidation. *APPLIED PHYSICS, Vol. 12, No. 2*, 155-164.

Bullock, P. J. (2008). The easy button for driven pile setup: dynamic testing. In *From Research to Practice in Geotechnical Engineering* (pp. 471-488). Gainesville, FL.

CFEM. (2006). *Geotechnical Design of Deep Foundation.* Calgary: Canadian Geotechnical Society.

Cryer, R. (1963). A comparison of three-dimensional theories of Biot and Terzaghi. *The Quarterly Journal of Mechanics and Applied Mathematics, Volume 16, Issue 4*, 401-412.

Fakharian, K. A. (2013). Contributing factors on soil setup and the effects on pile design parameters. *Proceedings of the 18th International Conference on Soil Mechanics and Geotechnical Engineering*, (pp. 2727-2730). Paris.

Farsakh, M. (2015). Evaluating pile installation and subsequent thixotropic and consolidation effects on setup by numerical simulation for. *NRC Research Press*.

Gates, M. (1957). Empirical formula for predicting pile bearing capacity. *Civil Engineering Vol. 27, No. 3*, 65-66.

GRL-WEAP. (2010). Wave Equation Analysis Program. Developed by GRL Engineers Inc., Cleveland, Ohio.

Guo, W. D. (2000). Visco-elastic consolidation subsequent to. *Computers and Geotechnics 26*, 113-144.

Hannigan, P. G. (1998). *Design and construction of pile foundations Volume 1.* Washington, D.C.: National Highway Institute.

Haque, M. (2014). *A case study on instrumenting and testing full-scale test piles for evaluating set-up phenomenon.* Washington, D.C: Transportation Research Board Annual Meeting.

Ko, J. (2016). Large deformation FE analysis of driven steel pipe piles with soil plugging. *Computers and Geotechnics 71*, 82-97.

Linkins, G. R. (2004). Correlation of CAPWAP with Static Load Test. *Seventh International Conferece on the Application of Stress Wave Theory*, (pp. 153-165). Kuala Lumpur, Malaysia.

Mandel, J. (1953). Soil Consolidation (Mathematical Study). *Geotechnique*, 3:287-99.

Ng, K. W. (2011). *Pile setup, dynamic construction control and load and resistance factor design of vertically loaded steel H-piles.* Ames, Iowa: Iowa State Universtiy.

ParklandGEO. (2018). WEAP and PDA Testing. Calgary, AB: Parkland Geotechnical Consulting Ltd.

Randolph, M. (1979). Driven piles in clay - the effects of installation and subsequent consolidation. *Geotechnique 29 No.4*, 361-393.

Rausche, F. G. (1985). Dyanmic detemination of pile capacity. *Journal of the Geotechnical Division, ASCE*, Vol 111, Issue 3, 367-383.

Rice, H. B. (1976). *A Slug Test for Determining Hydraulic Conductivity of Unconfined Aquifers With Completely or Partially Penetraing Wells.* Phoenix, Arizona: Water Resources Research.

Roscoe, K. (1968). On the generalized behavior of 'wet' clay. *Engineering Plasticity*, (pp. 535-609). Cambridge.

Rosti, F. (2016). Development of analytical models to estimate pile setup in cohesive soils based on FE numerical analyses. *Geotech Geol Eng*, 1119-1134.

Smith, E. (1960). Pile driving analysis by the wave equation. *Journal of the Soil Mechanics and Foundations Division, ASCE, Paper No. 3306 Vol. 127 Part 1*, 1145-1193.

Terzaghi, K. (1925). *Erdbaumechanik auf Bodenphysikalischer Grundlage. Franz Deuticke,.* Liepzig-Vienna.

Wong, T. (1998). A numerical study of coupled consolidation in unsaturated soils. *NRC Canada*, 926-937.

Yellow Map. (2017). *Map of Alberta*. Retrieved from Yellow Map.

9.0 APPENDIX – RESULTS OF UNDRAINED TRIAXIAL COMPRESSION TESTS

CONSOLIDATED-UNDRAINED TRIAXIAL COMPRESSION TEST ON COHESIVE SOILS

ASTM D4767

PROJECT: Detailed Tank Geo
PROJECT#:
CLIENT:

SAMPLE ID: 2U2 at 10.7 m
SAMPLE DATE: February, 2016
TEST DATE: March 7, 2016

SOIL DESCRIPTION: Clay (Silty)

SAMPLE CONDITION: Undisturbed

HYDROMETER, LIMITS & PROCTOR	
Gravel	0.00%
Sand	3.10%
Silt	50.60%
Clay	46.30%
Liquid Limit	39.00
Plastic Limit	18.00
Optimum Moisture Content	-
Standard Proctor Maximum Dry Density (kg/m^3)	-

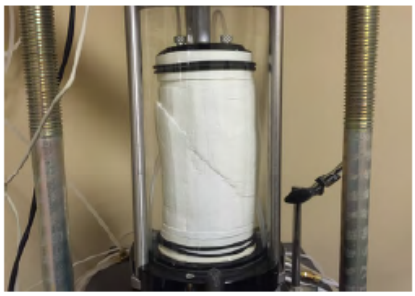

		POINT 1		POINT 2		POINT 3	
		INITIAL	POST-CONSOLIDATION	INITIAL	POST-CONSOLIDATION	INITIAL	POST-CONSOLIDATION
SPECIMEN MEASUREMENTS	Diameter (mm)	72.26	71.98	72.74	72.55	73.13	72.85
	Height (mm)	166.8	167.8	164.3	164.8	162.2	163.0
	D:H Ratio	2.3:1	2.3:1	2.3:1	2.3:1	2.2:1	2.2:1
	Area (mm^2) *Method A used post-consolidation.	4101	4069	4156	4134	4200	4168
	Volume (mm^3)	683891	682735	682735	681261	681261	679337
	Weight (g)	1348.6	1347.4	1347.4	1346.0	1346.0	1344.0
SOIL PROPERTIES	Moisture Content (%)	27.9%	27.8%	27.8%	27.6%	27.6%	27.4%
	Wet Density (kg/m^3)	1972	1974	1974	1976	1976	1978
	Dry Density (kg/m^3)	1542	1545	1545	1548	1548	1552
	Assumed Specific Gravity	2.71		2.71		2.71	
	Void Ratio	0.75	0.75	0.75	0.75	0.75	0.74
	Degree of Saturation	100%	100%	100%	100%	100%	100%
TEST PARAMETERS	Method for Saturation	Wet		Wet		Wet	
	Cell Pressure (kPa)	379		475		571	
	Back Pressure (kPa)	277		277		173	
	Effective Consolidation Stress, σ_3 (kPa)	103		198		398	
CONSOLIDATION	t_{50} (min)	21		18		20	
	t_{90} (min)	-		-		-	
	Shear Rate (mm/min)	0.032		0.037		0.033	

CONSOLIDATED-UNDRAINED TRIAXIAL COMPRESSION TEST ON COHESIVE SOILS

ASTM D4767

PROJECT: Detailed Tank Geo
PROJECT#:
CLIENT:

SAMPLE ID: 2U2 at 10.7 m
SAMPLE DATE: February, 2016
TEST DATE: March 7, 2016

SUMMARY OF TEST RESULTS		POINT 1	POINT 2	POINT 3
	Failure Criterion	Max. Deviator Stress	Max. Deviator Stress	Max. Deviator Stress
	Axial Failure Strain, ε_f (%)	2.9%	2.4%	4.8%
	Axial Strain Rate (%/min)	0.02	0.01	0.01
	Young's Modulus, E_{50} (Mpa)	15.0	33.6	42.9
	Deviator Stress, $(\sigma_1 - \sigma_3)_f$ (kPa)	110	206	346
	Major Stress, σ_{1f} (kPa)	213	404	745
	Induced pore-water pressure, Δu_f (kPa)	42	92	211
	Effective Minor Stress, σ'_{3f} (kPa)	60	106	188
	Effective Major Stress, σ'_{1f} (kPa)	170	312	534
	Correction for Rubber Membrane, $\Delta(\sigma_1 - \sigma_3)$ (kPa)	1.4	1.2	2.3
	Correction for Filter Paper Strips, $\Delta(\sigma_1 - \sigma_3)$ (kPa)	9.5	9.4	9.4
	Corrected Deviator Stress, $\sigma_1 - \sigma_3$ (kPa)	99	195	334

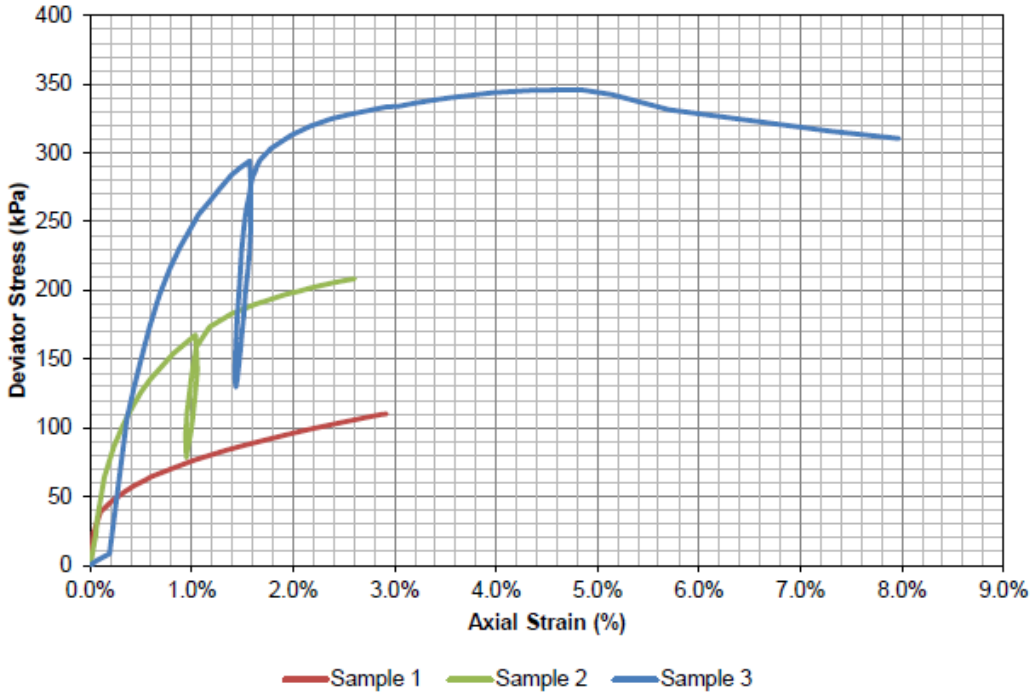

CONSOLIDATED-UNDRAINED TRIAXIAL COMPRESSION TEST ON COHESIVE SOILS

ASTM D4767

PROJECT: Detailed Tank Geo
PROJECT#:
CLIENT:

SAMPLE ID: 2U2 at 10.7 m
SAMPLE DATE: February, 2016
TEST DATE: March 7, 2016

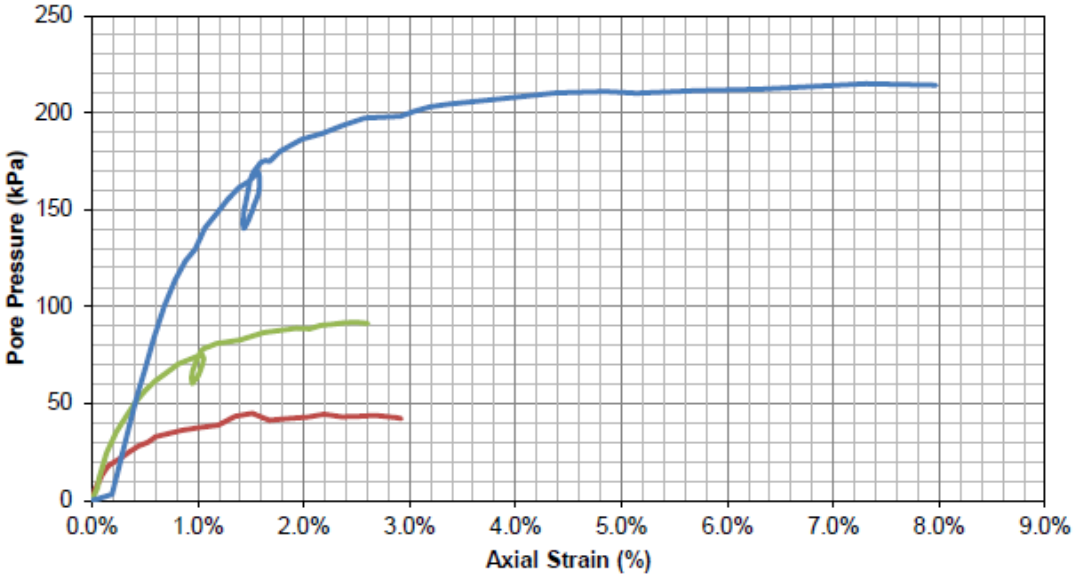

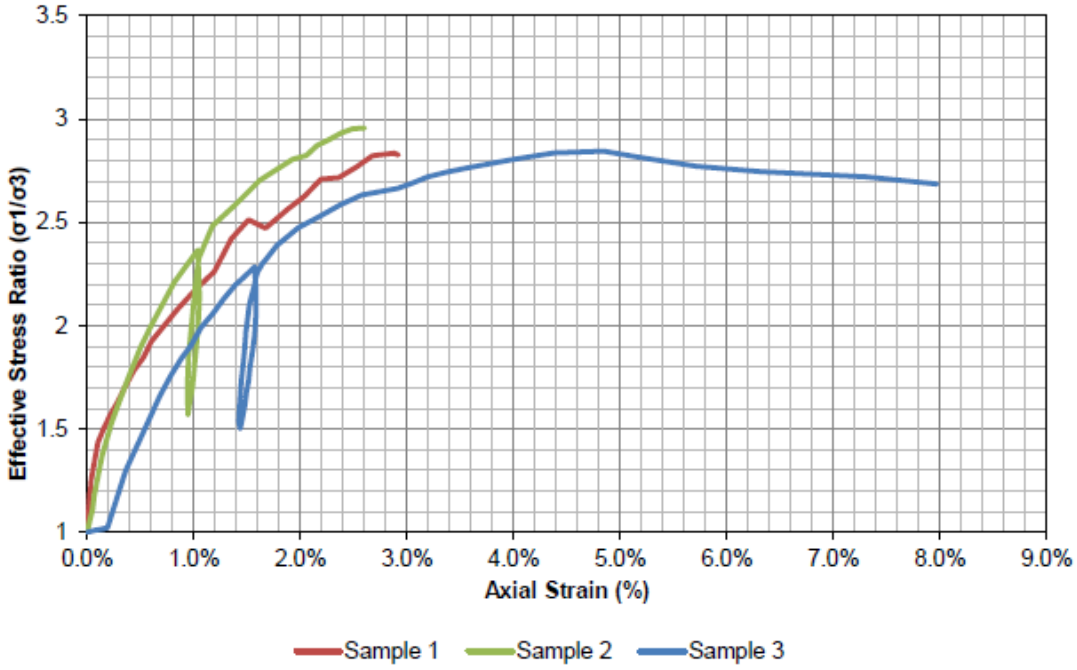

CONSOLIDATED-UNDRAINED TRIAXIAL COMPRESSION TEST ON COHESIVE SOILS

ASTM D4767

PROJECT: Detailed Tank Geo
PROJECT#:
CLIENT:

SAMPLE ID: 2U2 at 10.7 m
SAMPLE DATE: February, 2016
TEST DATE: March 7, 2016